Convective Distribution of Tropospheric Ozone and Tracers in the Central American ITCZ Region: Evidence from Observations During TC4

Author List: Melody Avery, Cynthia Twohy, David McCabe, Joanna Joiner, Kurt Severance, Eliot Atlas, Donald Blake, Paul Bui, John Crounse, Jack Dibb, Glenn Diskin, Paul Lawson, Matthew McGill, David Rogers, Glen Sachse, Eric Scheuer, Anne M. Thompson, Charles Trepte, Paul Wennberg, Jerald Ziemke

Submitted to the
Journal of Geophysical Research, Atmospheres
TC^4 Special Issue

October 25, 2009

Abstract:

During the Tropical Composition, Clouds and Climate Coupling (TC4) experiment occurring in July and August of 2007, extensive sampling of active convection in the ITCZ region near Central America was performed from multiple aircraft, satellite and balloon-born sensors. As part of a sampling strategy designed to study cloud processes, three NASA airplanes were repeatedly flown in formation to sample convective cells and outflow in the Eastern Pacific just south of Costa Rica and Panama. The ER-2, WB-57 and DC-8 flew in stacked "racetrack patterns" in convective cells, with remote-sensors located on the ER-2 and mainly *in situ* probes at two different altitudes on the WB-57 and DC-8. On July 24, 2007, the ER-2 and DC-8 probed an actively developing storm and the DC-8 was hit by lightning. We examine DC-8 *in sit*u data from this flight, and a second case study of convective outflow on August 5, 2007. The *in situ* data from extensive sampling in active convection reveals a significant anti-correlation between *in situ* ozone and condensed cloud water content. Further, since there is little variability in boundary layer ozone, and a vertical gradient in ozone, low ozone in the upper troposphere (500 – 150 hPa) can be used to indicate convective transport. As a result of the large spatial and temporal variability in surface CO and other trace gas emissions in this region, low ozone in the upper troposphere is a better convective indicator than pollution tracers. The correlation and distribution of lower tropospheric tracers methyl hydrogen peroxide, total organic bromine and calcium substantiates the evidence from ozone. A map of OMI measurements of mean upper tropospheric ozone in the vicinity of active convection show the distribution of lower ozone in the outflow regions of convective storms.

Statistical distributions and a simple mass balance calculation using data from all the DC-8 racetrack pattern sampling in the upper troposphere are used to estimate the amount of convective turnover that has occurred below the tropical tropopause transition layer (TTL) to be 50%, with an altitude of maximum convective outflow located between 10-11 km. This is lower than the 12 km altitude of maximum mass flux divergence predicted by theory, but is about 4 km below the tops of the cirrus anvils. It appears that convective lofting in this region of the ITCZ is either a two-stage or a rapid mixing process, because undiluted boundary layer air (ozone ~ 20 parts per billion by volume) is rarely sampled in the convective outflow.

1. Introduction:

1.1 TC4 mission and goals of this paper

This paper describes observations of trace gas redistribution by convection in the tropical troposphere, in the vicinity of the inter-tropical convergence zone (ITCZ) in the Gulf of Panama near Central America. Observational process studies to characterize vertical tracer transport and associated chemistry in strong tropical convection are needed to understand carbon and nitrogen budgets, and the oxidizing capacity of the atmosphere. Although convection is the dominant process controlling tropical tracer distribution, chemical transport models have difficulty simulating convective transport and chemistry accurately due to the dominance of small-scale diabatic processes. It is important to accurately quantify transport and chemistry of chemical tracers in the tropics because there is an abundance of energy available for phase transformation and photochemistry, and there is strong coupling between chemistry, clouds and climate impacts. Finally, the planetary boundary layer has the most potential for direct impact on the stratosphere in the tropics.

The measurements described here were taken from the NASA DC-8, ER-2, balloon sondes and the NASA Aura satellite during the Tropical Composition, Cloud and Climate Coupling Experiment (TC4), July 17 – August 8 of 2007. TC4 science goals, flight planning and flight summaries are described in the TC4 overview paper by Toon et. al. [2010]. The TC4 mission included sampling from the DC-8 as a moderate altitude platform, from the WB-57 for higher altitude sampling in the tropical transition layer (TTL, from 12-17 km) just below the stratosphere, and highest altitude sampling from the ER-2 with remote sensors similar to many found on NASA Earth Observing System (EOS) satellites. Whenever feasible, aircraft flights were planned to be coincident with an EOS satellite overpass, in order to validate the satellite instrument observations, or to combine them with the suborbital *in situ* and remote measurements for analysis.

The scope of the TC4 mission included measurements to quantify cloud composition and physics, tropospheric and lower stratospheric composition and chemistry, and vertical transport by convection. In this paper we focus on addressing a few of the major TC4 science questions by analyzing data in the troposphere. These science questions are paraphrased below:

- "What is the composition of the tropical troposphere below the TTL?
- "What are the mechanisms that control ozone within and below the TTL?"
- "What is the chemical nature of the convective outflow?

1.2 Origin of ozone in the upper troposphere

Ozone is important for determining the oxidizing capacity of the atmosphere, and it is both an infrared and visible wavelength absorber, which either heats or cools the atmosphere locally, depending on altitude. Processes that control ozone in the tropical upper troposphere (500-150 hPa) are expected to be convective outflow from the boundary layer, extra-tropical advection, and *in situ*

photochemical production. The chemical lifetime for ozone loss is about 50 days in the tropical upper troposphere [*Folkins et al*., 2006], compared to the typical vertical mixing time of less than 1 day during TC4 [*Pfister et al*., 2010], so that ozone can be used as a dynamical tracer for vertical transport if *in situ* ozone production is not too large.

In situ ozone production can be enhanced by biomass burning plumes, or by NO produced by lightning. In the tropics there is generally plenty of water vapor and sunlight available to form reactive odd hydrogen-containing radicals ($OH+HO_2 \equiv HO_x$), and carbon monoxide or hydrocarbons from biomass burning are often available for oxidation and ozone production. However, ozone is also destroyed very effectively and catalytically by HOx, provided that the $OH:HO_2$ ratio favorable to ozone production is not maintained by the oxidation and cycling of NO and NO_2 radicals (NO_x). In general, ozone formation is NO_x -limited in the tropical TC4 study region. Lightning-produced NO_x can cause ozone production to increase downwind of electrically active convection. Direct production of ozone by lightning is difficult to measure, and apparently rare [Ridley, 2006].

Tracer sampling of the upper troposphere during TC4 mainly showed well-aged pollution, well mixed into a clean tropical background. Estimates of the ozone production rate range between 0.2 parts per billion by volume (ppbv)/hour expected from calculations published by *Folkins et al.* [1999], up to 0.5 ppbv per hour calculated during TC4 by Salawitch [plot not shown]. *Morris et al.* [2010] measured even higher ozone production rates of 3-10 ppb/hour between 2-5 km in a convective cloud. This suggests that *in situ* ozone production is occurring vigorously during vertical transport in convection and can be significant.

1.3 Meteorology during TC4 and vertical transport

The TC4 study area was chosen to be in the vicinity of the ITCZ so that the aircraft, balloons and satellite sensors could sample active convection [Toon et. al. 2010]. During July and August of 2007, SSMIS F16 rainfall images show that maximum rainfall from the ITCZ was located in the Gulf of Panama, in the center of the TC4 study area. Sea surface temperature anomalies in the Eastern Pacific were 1-1.5 degrees below average, indicating the onset of a moderate cold-phase ENSO event [NOAA Climate Prediction Center, Diagnostic Discussion]. Comparison with other years showed less convection and less intense convection during 2007 than usual [*Pfister et al.,* 2010], with stronger than usual easterlies in the upper troposphere that are typical of the cold phase of ENSO. Examination of the wind measurements during local sampling in the upper troposphere from the DC-8 using the Meteorological Measurement System (MMS) [*Scott et al., 1990*] confirms that >90% of the wind vectors have an easterly component.

Winds measured in the mid-troposphere during local flights on the DC-8 also almost always show an easterly component, with a slight bias to the south compared to the upper tropospheric winds. However, winds at the surface in the

planetary boundary layer are much more complex. Large-scale data analysis [*Pfister et al.,* 2010] and dust collected from low altitude sampling shows that the lower level winds brought air from Africa and South America into the boundary layer in the main TC4 study region, while vector winds measured on the DC-8 show winds coming from all 4 quadrants, and chemical tracers showed a mix of both polluted continentally-influenced air and very clean maritime air, as discussed below. While convection in the ITCZ region in 2007 was relatively weak, analysis by *Hlvaka et. al.* [2010] shows that the TC4 local study area was still very cloudy, with on average greater than 94% multilayered cloud cover, most frequently marine stratus decks overlain with cirrus from evolving convective anvils. Further, periods of active convection were sampled by the airplanes, particularly at the beginning and at the end of the mission.

In this paper we look at the impact of these dynamics on the composition of the upper troposphere in the TC4 study region. First we present an overview of the distribution and correlations of O_3, CO and CH_4, and focus on the composition of the boundary layer source region. Two case studies are presented during which the planes sampled active convection and convective outflow. These provide an opportunity to establish whether there are potentially robust tracer correlations in the extensive DC-8 data set in convectively influenced air. During these two flights, the inverse relationship between condensed cloud water content and ozone is the strongest we found in the fast-response *in situ* data set, so we test the larger ensemble of upper tropospheric data from the "racetrack" flights to see if this relationship appears to be true more universally. Since it does, we use this information to find the altitude of maximum convective outflow, and compare our results with ozonesonde data and with vertical boundary layer tracer distribution.

2. Observations and Methods of Analysis:

2.1 *In situ* data aircraft data

The *in situ* data that we use in this paper was taken from the NASA DC-8 and WB-57 by various investigators as described here. The list of chemical and physical data considered and analyzed in this paper includes ozone, carbon monoxide, methane, condensed cloud water content, organic bromine, peroxy nitric acid, calcium and methyl hydrogen peroxide. Other reactive nitrogen species are discussed more generally, but are not used for analysis because in this active convective region most reactive nitrogen species are not conserved, and these tracer relationships are chaotic.

The ozone, carbon monoxide, methane and condensed cloud water content data on the DC-8 are available at one-second-time resolution, corresponding to a horizontal resolution of about 200 m. The location of sampling for each of these constituents on the DC-8 is shown in Figure 5 of *Toon et al.* [2010]. Merged data files have been created, with all data aligned to the time stamp of water vapor data measured by the Langley DLH diode laser hygrometer, an open-path measurement without sample lag considerations. Ozone was measured using

fast-response nitric oxide chemiluminesence [*Gregory et al.* 1987, *Pearson and Stedman*, 1980]. Carbon monoxide and methane were measured using a tunable diode laser–based absorption technique by the Differential Absorption for CO Measurements (DACOM) instrument [*Sachse*, 1987]. For measurements of the condensed cloud water content (CWC) we used the bulk data from the NCAR counterflow virtual impactor (CVI) described by *Twohy et al.* [1997]. During the ER-2 and DC-8 flights that occurred on July 24, 2007, the plane flew through developing convective cores with large vertical velocities and corresponding CWC. CWC content derived from the SPEC 2DS cloud probe data [*Lawson et al.,* 2006] was used during this flight.

The Meteorological Measurement System (MMS) provided accurate, high resolution pressure, temperature and wind data used in this analysis for both the DC-8 and the WB-57, using instrumentation similar to that described for the ER-2 in *Scott et al.* [1990]. Ozone data from the WB-57 was measured using a dual beam ultraviolet photometer. We also compare the aircraft data with ozone data measured from sondes using electrochemical cells *Thompson et al.* and *Morris et al.* [2010].

We compared the vertical distribution of some other trace gases to our results from examining ozone. Methyl hydrogen peroxide (MHP) and PNA (peroxy-nitric acid) were measured using a chemical ion mass spectrometer (CIMS) technique developed at the California Institute of Technology [*Spencer et al*. 2009, *St Clair et al*. 2010]. Total organic bromine was calculated from individual species measured by analysis of whole air samples using gas chromatography at the University of Miami for the WB-57 and the University of California, Irvine for the DC-8. Calcium was analyzed from bulk aerosol composition measurements made from the NASA DC8 by the University of New Hampshire soluble acidic gases and aerosols (SAGA) instrument (*Dibb et al.*, 2003).

2.2 Suborbital and satellite-based remote data

Cloud images from the Cloud Physics Lidar (CPL) on the ER-2 were used to locate aircraft measurements from the DC-8 relative to the cloud top height and cloud morphology. The CPL cloud images are a time series of 532 nm attenuated backscatter profiles, measured as described in *McGill et al.* [2002]. During TC4 there were several near coincidences between overpasses by the CALIPSO satellite and the multiple-aircraft flight tracks, and we show a comparison between cloud images from the CALIOP instrument [*Winker et al.* 2007], the CPL on the ER-2 and in situ CVI measurements of CWC as a movie (see section 2.3, below).

We evaluate mean tropospheric ozone volume mixing ratios calculated between the tropopause and effective scene pressures derived using the NASA Aura OMI and Microwave Limb Sounder (MLS). The tropospheric ozone column residual is first determined by subtracting the MLS version 2.2 stratospheric column ozone

[*Froidevaux et al.,* 2008] from the OMI-TOMS [*McPeters et al.,* 2008] measured column ozone for each OMI pixel. This measured column does not include ozone that is shielded from the satellite by clouds. The MLS data are interpolated between orbits using a trajectory model as described by Schoeberl et al. [2007]. Ozone mean volume mixing ratio (units ppbv) is then calculated by multiplying the derived residual ozone column by 1270 and dividing by the difference between the tropopause and effective scene pressure (in hPa) [e.g., *Ziemke et al.*, 2001, *Joiner et al.,* 2009]. Tropopause pressure is derived from GEOS-4 analyses using the standard temperature lapse rate definition. The derived tropospheric column ozone includes a calibration correction of -5 DU that is based upon an analysis of tropical ozonesonde measurements [*Joiner et al.,* 2009]. This offset is consistent with a slight high bias in the MLS stratospheric column [*Froidevaux et al.* 2008] coupled with a low bias in the OMI-TOMS total column ozone [P. K. Bhartia, private communication, 2009]. The global correlation between the OMI/MLS-derived 200 hPa to surface column ozone and ozonesondes was 0.8 [*Joiner et al*., 2009].

2.3 Data synthesis and analysis strategy

In situ data from the DC-8 was merged as described above, with 1-second time resolution and a corresponding approximate horizontal resolution of 200 m. The DC-8 data set in the upper troposphere extends between 8.5 and 12.2 km, with a corresponding potential temperature range of 330-350 K. We created a DC-8 data ensemble from sampling during the local "racetrack" flights with a limited geographical domain between 4-10 N latitude, and between 79 – 87 W longitude. The flights used occurred on July 17, 22, 24 and 31, and August 3, 5, and 8 of 2007, and these are shown in Figure 1, with the DC-8 flight track colored by *in situ* ozone amount. The ER-2 flew as well on these days, with the degree of flight coordination increasing with practice as the mission progressed. Flight coordination is discussed extensively in *Toon et al.* [2010]. The WB-57 also flew a coordinated pattern during the August flights, and a next step in data analysis will be to compare data from these WB-57 flights.

Merging and interpreting the remote and in situ data together is challenging. We developed a special-purpose program to combine the CPL and CALIOP images and DC-8 data, as well as their geo-location and time stamp information, into geometry and scalar-data files compatible with the COTS 3-D Visualization software tool called "EnSight." These datasets could then be co-located in space and time, with respect to a map of the Earth built from the GTOPO30 digital elevation model (DEM) and the NASA Blue Marble cloud-free image. The visualization software provided both 3-D movies and stills of the combined data set, providing a powerful and intuitive way to spatially and temporally link the observations, and to build intuition for data analysis decisions. A movie showing the precise correspondence between a CALIOP cloud image from the August 5th CALIPSO overpass, the corresponding CPL cloud image from the ER-2, and in situ cloud water content from the DC-8 is shown at this link: http://tinyurl.com/tc4nasa-video01. The vertical scale is expanded, in order to

visualize detailed structures. The movie was submitted with this paper, and upon review will be archived with it.

3. Results and Discussion:

3.1. Overview of *in situ* observed tropospheric composition

To provide an overview of the larger context of the background tropical tropospheric chemical composition of the tropical tropospheric study area, we have plotted the aggregate median vertical profile and statistical distribution of ozone and carbon monoxide, shown as Figure 2. We look at ozone and carbon monoxide because both gases are not significantly soluble in the cloudy tropical environment, and they both have similar chemical lifetimes of about 50-60 days, much longer than the vertical mixing time of less than 1 day. The tracer data is binned at 1 km resolution, and includes all of the measurements from the DC-8 between 7S and 17 N latitude, and between 70 – 90 W longitude.

The median ozone profile shows a characteristic tropical "S"-shape [*Folkins,* 2002], with depleted ozone in the boundary layer, some ozone enhancement in the middle troposphere, a minimum caused by convective outflow in the upper troposphere, between 9-10 km, and a monotonically increasing ozone gradient above the outflow maximum. In the upper troposphere, enhanced ozone of more than 65 ppbv occurs in less than 25% of the data, except above 12 km, with potential temperatures approaching or greater than 350K. Based on this, in this paper when we refer to "high" ozone, we mean specifically ozone concentrations greater than 65 ppbv. Ozone in the boundary layer is both low and strikingly uniform throughout the sample region. Correlation during boundary layer sampling with MMS wind measurements shows that ozone measured while winds have an easterly component (60 – 110 degrees) has the smallest range (19-25 ppbv), while ozone measured while winds have a southerly or westerly component has a slightly wider range (12-28 ppbv). A probability distribution of boundary layer ozone shows the median value to be about 21 ppbv, with less than 10 ppbv of variability everywhere, and no significant difference (0.5 ppbv) between the Atlantic and the Pacific marine boundary layers. This suggests that catalytic destruction of ozone by reactive hydrogen radicals (HOx) removes ozone efficiently in the lowermost atmosphere. This appears to be the case in both the marine boundary layer, and in measurements over land. Comparison with the more polluted NATIVE surface ozone data set from Las Tables, Panama [Figure 10, *Thompson et al*., 2010] also shows surface ozone averages near 20 ppbv.

The carbon monoxide median profile is very uniform vertically, with medians between 70-90 ppbv throughout the troposphere. This contrasts with the large range of CO measured in the boundary layer, between 55-155 ppbv with the 75th quartile occurring at 90 ppbv. An examination of DACOM measurements of CO at take-off and landing at Alajuela airport shows a large amount of day-to-day variability, despite its proximity to San Jose. Comparison of the aircraft CO

353 measurements by DACOM with surface measurements of CO from the NATIVE
354 trailer in Panama show that the Panama site was relatively polluted, since 75% of
355 the boundary layer aircraft measurements show CO of 90 ppbv or less, while all
356 of the NATIVE data indicates CO of 90 ppbv or more.
357
358 Carbon monoxide is usually the product of incomplete combustion, but the
359 convectively active TC4 region does not show much fresh pollution or biomass-
360 burning enhancement. This is substantiated by measurements of HCN, a
361 biomass burning tracer that is also not enhanced above a moderate background
362 level in the convective area. The relationship between ozone and carbon
363 monoxide is complex, and varies by flight day. Positive correlations can indicate
364 aged pollution or very clean air; negative correlations can indicate stratospheric
365 influence, *in situ* ozone production from lightning NO_x, biogenic influence, or
366 fresh smoke. Because of these ambiguities, it is difficult to use the correlations
367 to provide much useful information about air mass history. CO is not a useful
368 tracer for convective transport because of the lofting of both clean and dirty
369 boundary layer air by convection. During the convective "racetrack" flights, either
370 a positive or a negative correlation tends to persist for all altitudes sampled,
371 reflecting the influence of either a clean or a polluted boundary layer. A
372 composite correlation plot for the mission shows weak or no correlation,
373 indicating that a large amount of mixing has occurred in this region.
374
375 For context, in Figure 3 we look at the vertical ozone distribution during TC4
376 compared with ozone measured at similar latitudes during other aircraft field
377 missions. The comparison is facilitated because these measurements were all
378 made using NASA Langley NO chemiluminesence detectors, with an estimated
379 3% accuracy [*Avery et al.,* 1999, *Gregory et al.,* 1987, *Pearson and Stedman*,
380 1980] All but the ABLE-2B mission occurred during a mild ENSO cold phase.
381 The figure shows the median ozone concentration measured in 1 km bins as a
382 function of altitude. We show the ABLE-2A and 2B missions, with sampling over
383 the Amazon basin and Western Atlantic, the PEM Tropics A and B (PTA and
384 PTB) missions with pan-Pacific tropical sampling, and the TRACE-P mission,
385 which featured Asian air pollution and sampling of the Western Pacific.
386
387 The largest difference in tropospheric ozone appears to be seasonal, with
388 roughly double the amount of ozone occurring in the boundary layer during the
389 summer or fall than during springtime. This seasonal difference persists in the
390 middle and upper troposphere. There was about 10 ppbv more ozone measured
391 during TC4 in July-August than there was during PTA in August-September,
392 most likely due to the difference between sampling the remote Pacific and the
393 TC4 study area around Central America. The TRACE-P mission was unusual in
394 targeting Asian pollution, with a resulting high mid-tropospheric ozone median.
395 Unfortunately, the ABLE-2A measurements do not extend higher than 5 km, but
396 these show that ozone was a bit lower in the lower troposphere over the Amazon
397 basin than measured during TC4. This may be because the tropical rainforest is
398 a very efficient sink for ozone. This was discussed in detail by Gregory et. al.

399 [1988], describing the ABLE-2A measurements. Our TC4 measurements from a
400 boundary layer leg over the Peruvian rain forest substantiate this, with the lowest
401 average ozone concentration measured during TC4 (11 ppbv) and the highest
402 CO (153 ppbv).
403
404 Methane and ozone from TC4 are shown in Figure 4. These are mainly
405 uncorrelated, with the exception of two plumes containing very high biogenic
406 methane sampled in the Colombian boundary layer, once over land, and once
407 just off the Pacific coast. The distribution looks very similar to ozone correlations
408 with CO, and this plot is shown to illustrate the well-mixed state of the free
409 troposphere during TC4. Methane concentrations measured at the NOAA CMDL
410 ground stations in the Northern and Southern Hemisphere (NH and SH) closest
411 to the TC4 sample region are shown on the plot for comparison. This plot
412 suggests that almost all of the air sampled during TC4 came from the tropical
413 NH, with only 4% of air sampled having methane amounts less than 1750 ppbv,
414 indicating no significant unmixed stratospheric or SH air was sampled aside from
415 that in one plume on August 6, the low methane "tail" in the figure. *Pfister et al.*
416 [2010] estimate that only 10-30% of air sampled in the troposphere during TC4
417 comes from the NH mid-latitudes poleward of 25 N during the mission, which is
418 consistent with this tracer data.
419
420 Comprehensive reactive nitrogen measurements (NO, NO_2, HNO_3, PAN, PNA)
421 were made from the NASA DC-8 during TC4, and we consider them here. In mid-
422 latitudes near convection, *Bertram et al.* [2007] have reported a compelling
423 relationship between the NO_x/HNO_3 ratio in an air parcel and the time since
424 convection lifted the air from the lower into the upper troposphere. One would
425 expect HNO_3 to be scrubbed out of air that has been transported upwards
426 through a cloud, and with the addition also of lightning-produced NO_x one
427 expects the NO_x/HNO_3 ratio in very fresh convective outflow to be large. With
428 time, much of the NO_x will be converted into HNO_3 through oxidation and gas-
429 phase HNO_3 can be released by cloud droplet evaporation. During TC4,
430 *Scheuer et al.* [2010] found that HNO_3 was depleted on ice crystals in cirrus, and
431 that it was enhanced in a thin layer just below cirrus by sedimenting and
432 sublimating particles. In clouds, HNO_3 is strongly anti-correlated with CWC,
433 because it is soluble (plot not shown). Because of the frequency of both
434 convection and occurrence of cirrus during TC4, and the non-conservation of
435 HNO_3, the air parcel "age' since convection cannot be determined using the
436 *Bertram et al.* [2007] method. It is likely that this method works much better in
437 mid-latitudes than in the tropics.
438
439 Further examination of the NO_2/NO_x ratio using NO_2 data from OMI and lightning
440 data by *Bucsela et al*. [2010] suggests that lightning NO_x enhancement can be
441 between 1.5-2.5 times the NO_x background, but there is also less lightning NO_x in
442 tropical convection than in thunderstorms that are associated with mid-latitude
443 fronts. The upper tropospheric relationship of NO_x with O_3 is uncorrelated,
444 indicating that the production of new ozone from lightning NO_x might happen

445 downstream, but is not a dominant process in TC4 maritime convection. While
446 the ratio of total reactive nitrogen (NO_y) to ozone has been used to indicate
447 ozone production potential [*Ridley,* 2006], in the actively convective TC4
448 "racetrack" region the NO_y/O_3 ratio is also uncorrelated (like NO_x/HNO_3, plot not
449 shown), and is not useful for data interpretation here. PAN observations in the
450 TTL [Elkins, plot not shown] suggest that a significant amount of PAN (greater
451 than 30 ppt) is vertically transported out of the boundary layer into the upper
452 troposphere. Because PAN is not water-soluble and does not deposit on ice
453 particles, this is likely the dominant way for reactive nitrogen to be transported
454 vertically into the TTL and horizontally in the upper troposphere.
455
456 **3.2. Case studies of convective transport**
457
458 **3.2.1 July 24, 2007, the "Thor" flight**
459 On the morning of July 24, 2007, the DC-8 and the ER-2 were to sample a
460 developing thunderstorm complex in the ITCZ system at about 5 deg N, 85 deg
461 W. The DC-8 was to extensively sample the boundary layer in the actively
462 developing storm, and then to ascend through the storm and to sample cirrus in
463 the outflow region to characterize convective transport and mixing. Although the
464 flight was a success, it was cut short by a lightning strike to the DC-8. Because
465 of the potential danger of another lightning strike, this was the only flight during
466 the TC4 mission that sampled the core of an actively developing storm.
467
468 A Geostationary Operational Satellite (GOES) visible satellite image overlain with
469 the ER-2 and DC-8 flight tracks is shown in Figure 5a. The prevailing wind in the
470 cirrus anvils of the convective cells is NE at 40 kt, and one can see this in the
471 cloud pattern. One can also see the more orderly "race track" pattern flown by
472 the ER-2 above the cirrus, as opposed to the flight pattern taken by the DC-8
473 after it was hit by lightening. The cloud physics lidar (CPL), making
474 measurements from the ER-2, provides context for the DC-8 *in situ*
475 measurements taken inside the convective cell. Figure 5b shows a three-
476 dimensional CPL image of the cirrus anvil, and the coincident DC-8 flight track,
477 colored by *in situ* ozone concentration. Ozone was 20-25 ppbv in the boundary
478 layer beneath the storm, typical during TC4, increasing to 30-35 ppb at 3-4 km,
479 as expected. The CPL shows that the cirrus cloud tops extend to 14-15 km, so
480 the DC-8 in cloud sampling occurred about 3-4 km below the tropopause. One
481 can see that the cirrus are ragged and uneven, and that the ozone inside them is
482 highly variable, between 30 and 75 ppbv.
483
484 While the CPL and DC-8 flight track image shows the relative location of *in situ*
485 sampling to the cirrus cloud anvil of the developing storm, a time series of
486 measurement correlations is needed to establish the cause of so much variability
487 in the ozone. Figures 5c and 5d show the time series for the entire flight (5c) and
488 for sampling from 54440-56320 UT seconds (5d) while the DC-8 was inside the
489 anvils at 11 km, 225 hPa, and penetrated the core of the storm where the
490 ambient temperature was -47 degrees C, so the cloud particle phase was ice.

The first set of time series shows CWC, ozone, carbon monoxide and altitude. The CVI instrument, while normally accurate to within 15% (Twohy et al., 1997), relies on subisokinetic enhancement of condensed water to measure low concentrations, and requires manual adjustment to measure high water contents such as are present in convective cells. Since these were not anticipated for the July 24th flight, the CVI signal was saturated twice during the flight when the DC-8 passed through convective turrets. The 2DS cloud probe measured the large spikes in condensed water content (Figure 6) during these periods. The 2DS integrates the cloud particle size distribution to obtain condensed water and this technique generally agreed well with the CVI measurement during the rest of the TC-4 mission. There is a striking anti-correlation between CWC and ozone, with high ozone values (65-70 ppb) measured where CWC is low ("no cloud"), and lower ozone values (30-35 ppbv) measured inside the clouds. Positive vertical winds (Figure 6) and upwelling radiance measured during this flight (not shown) are also anti-correlated with ozone. This strong anti-correlation between ozone and clouds persists throughout the TC4 data set.

There is a positive correlation during this flight between carbon monoxide and ozone, indicating some aged pollution in the upper tropospheric background air, and vertical advection of relatively clean lower tropospheric air. However, this result is not consistent during upper tropospheric sampling on other flights. Correlations between ozone and horizontal wind direction, and between ozone and oxides of nitrogen are not significant during this flight (not shown), nor are they significant during the "racetrack" sampling in the upper troposphere for the mission as a whole. This indicates that convection dominates in redistributing ozone, and in this region it is more significant as a process for creating ozone variability than horizontal advection and *in situ* photochemistry.

Figure 6 shows ice water content measured by the 2DS probe during a segment of this flight when the DC-8 sampled actively developing convective cores. The figure also shows MMS vertical velocity of 20 m/s. A simple calculation of ozone production is possible in this very fresh convection. If ozone production rates of 3-6 ppbv/hour are used, as measured by *Morris et al.* [2010], and 10-20 m/s is used for the range of vertical velocity over a representative distance of 8000 m, only 0.4-1.6 ppbv of ozone can be made during vertical transport. This indicates that the 10 ppbv difference between the low O_3 mixing ratios of 30-35 ppbv measured in the convective cloud and boundary layer O_3 was not likely to have been produced during vertical transport. The higher O_3 mixing ratios indicate that this air was also not transported directly from the boundary layer to 10-11 km (225 hPa), where our sampling occurred.

While relatively low ozone concentrations in the upper troposphere can be an effective indication of convective influence, this argument needs to be complemented by examining concentrations of a "positive" tracer for convection. Methyl hydrogen peroxide (CH_3OOH, MHP) is a convenient convective tracer to use in this case, because it is enhanced in the lowermost atmosphere but it is not

significantly soluble. *Cohan et al.* [1999] have shown that MHP in very fresh convection can be elevated up to 6 times over the upper tropospheric background, but decays in the upper troposphere with a chemical lifetime of 1-2 days.

Figure 7 shows CO, O_3, MHP and pernitric acid, (NO_2HO_2,PNA) measured during two of the 11 km (225 hPa) sampling loops, along with averages obtained just prior to the ascent during the boundary layer run. The addition of the tracers shows that three distinct air types were sampled. Air that has recently been transported into the upper troposphere with low O_3 has high MHP and low PNA. This freshly convected air can be seen at 5.37e4 and 5.46e4 GMT sec, corresponding to the DC-8 passage through convective turrets shown in Figure 6. The second air type, background tropospheric air with high O_3 mixing ratios (> 60 ppb) has relatively high PNA and low MHP, with examples centered near 5.39e4 and 5.44e4 GMT seconds on the plot. There are also slightly higher values of CO and CH_4 (not shown) that are anti-correlated with O_3, with examples at around 5.50e4 and 5.63e4 GMT sec on the plot.

Figure 8 maps the flight track, indicating the location of these different air types. These have spatial scales of the order of 10-50 km. Figure 8 also shows approximate footprint sizes of various ultraviolet and visible satellite backscatter instruments. The smallest is that of the Ozone Monitoring Instrument (OMI) that flies on NASA's Aura satellite [*Levelt et al., 2006*]. Its nadir pixel is approximately 12 km x 24 km. It has been used to retrieve ozone mixing ratios inside deep convective clouds [*Ziemke et al., 2009*]. The spatial scales of the different observed air types are similar to the OMI nadir footprint, so it is feasible that OMI data can resolve ozone variability that is caused by convective processes.

The mean tropospheric ozone volume mixing ratios (units ppbv) calculated between the tropopause and effective scene pressures (300-450 HPa) derived using the NASA Aura OMI and Microwave Limb Sounder (MLS) are shown in Figure 9a for the AURA overpass occurring closest to this flight (18:30 Z on July 24, 2007). This overpass occurred about 4 hours after the DC-8 sampled inside the developing convection as described above. Examination of GOES images using loops provided by the Langley TC4 satellite group (*Minnis,* 2010) shows that during this time the convective system continued to grow, with outflow streaming off to the southwest. Figure 9b shows a GOES IR color-enhanced image that corresponds most closely to the AURA overpass. The DC8 flight path while the plane was circling near the tops of the convective clouds is shown in 9a (OMI plot). On this day, the OMI pixels over this area correspond to the west side of the swath where the pixels are significantly larger than the near-nadir pixels seen to the east. In this area there is a large contrast in mean ozone mixing ratios from < 40 ppbv (blues) to >65 ppbv (reds).

These derived OMI column-mean mixing ratios appear to be consistent with the in situ measurements taken several hours earlier in the developing storm,

showing the contrast between ozone mixing ratios in freshly lofted and background upper tropospheric air. As expected, OMI/MLS data does not capture the finer-scale ozone variability shown in the *in situ* measurements. However, the larger perspective that OMI offers clearly shows the extent of lowered ozone in the convective outflow to the southwest of the system. This is also captured by OMI for other convective areas visible in this region, with another example visible in the Caribbean just north of Panama. A histogram of the OMI mean tropospheric ozone measurements for the entire region peaks at 49 ppbv (+/- 10 ppbv), which is consistent with the *in situ* ozone distribution shown in Figure 2a, and is indicated in the clear regions of Figure 9a. Since sonde and lidar ozone data is not available in deep convective clouds, this comparison of *in situ* and OMI ozone measurements provides a unique validation of the OMI/MLS mixing ratios derived inside convection.

3.2.2 August 5, 2007, Convective Outflow

On this day DC-8, ER-2 and WB-57 flew a well-coordinated pattern in convective outflow, first identified in satellite images. In section 2 we presented a movie showing the relationship between the DC-8 flight track and the cirrus outflow from the convection sampled, including mages of the cirrus from both the CALIOP instrument on CALIPSO and the CPL. Figure 10 focuses on measurements from the DC-8. Panel a shows a 3-dimensional picture of the CPL cirrus image and in-situ ozone data (bottom) and the *in situ* carbon monoxide data (top). During this flight the boundary layer and lower troposphere are quite polluted compared with the July 24th flight shown above, and on this day, O_3 and CO are almost always anti-correlated.

The 3-dimensional picture shows that the highest DC-8 racetrack pattern was flown inside the cirrus, 3-4 km below the anvil tops at 14-15 km. Panel b shows the O_3, CO and CWC traces from the racetrack sampling. The spikes of higher ozone (60 ppbv) coincide with lower CO (90 ppbv) on the side of the racetrack where the DC-8 turns around outside of the cloud, as indicated by the absence of CWC. This trace is shown because it is a good example of vertical advection of polluted air out of the boundary layer, and of the in cloud/out of cloud difference in composition. Panel c is a plot of O_3 (y-axis) vs. CWC (x-axis) from the whole flight, and points with CWC > 0.1 g/m3 are colored red to emphasize the thickest clouds. It is interesting to note the predominance of O_3 concentrations of ~ 25 ppbv in the lower clouds, and O_3 ~ 35-40 ppbv in the anvil clouds. This suggests that convection transports air from above the boundary layer, from 2-3 km, into the upper troposphere, but does not loft the boundary layer directly.

3.3 Regional statistics

In this section we look at the combined data set from all of the local upper troposphere (8-12 km) sampled during TC4. Figure 11 shows the O_3:CWC relationship in all the data, with the thickest clouds (CWC > 0.2 g/m3) colored in red. The cloudy areas clearly have less ozone than the clear ones, with all of the high ozone occurring where CWC approaches zero. A somewhat arbitrary value

of 0.01 g/m^3 was chosen to divide the data set into "cloudy" and "not cloudy" bins for looking at ozone probability distributions. The CVI out-of-cloud baseline is lower than this (~0.002 g/m^3), but a higher value is chosen to avoid including a CVI cloud exit hysteresis signal as a cloud. The ozone distribution is not very sensitive to this choice, tested between 0.002 – 0.02 g/m^3.

Figure 12 a and b shows the "in cloud" and "out of cloud" probability histograms of ozone and carbon monoxide. The peak of the in-cloud probability distribution occurs at 37 ppbv, which is representative of in-cloud O_3 mixing ratios measured in both active convection and convective outflow as shown above. There are relatively few measurements of O_3 between 50-75 ppbv in the cloudy data. The small peak in O_3 at 80 ppbv in cloud did not reach the upper troposphere by vertical transport directly from the lower troposphere, because there were no measurements of ozone greater than 75 ppbv below 10 km. The DC-8 must have flown through a small, cloudy pollution plume, but there are so few data points that this small plume does not affect our conclusions significantly.

In contrast, the "out of cloud" ozone measurements in the upper troposphere show ozone concentrations between 50-75 ppbv in about 50% of the air sampled. The CO histograms show a peak in "clean" air with CO of 75 ppbv outside of the clouds, perhaps representing a tropical upper tropospheric background. There is a somewhat more even distribution of CO occurring in clouds, reflecting the large amount of variability in CO in the lower troposphere. The cloudy air contains more CO than the clear air, indicating that vertical convective transport is a net source of "dirty" air to the upper troposphere.

3.4 Comparison with sondes and tracer profiles

An analysis of vigorous tropical convection in the Western Pacific by *Solomon et al.* [2005] documents the transport of air containing very low ozone to the tropical TTL region, and also shows the usefulness of examining a profile of low ozone measurements for establishing the altitude of maximum convective outflow. From our analysis of in cloud and out of cloud probability distributions of ozone measured in the upper troposphere, we find a minimum in the histogram occurring at 44 ppbv, with a sharp peak in the cloudy mixing ratios below this value. Using this number as a threshold for "low ozone", we calculate the fraction of measurements of low ozone in 500 m bins throughout the troposphere for the Panama and Alajuela sondes, as well as for the WB-57 and DC-8 local ozone profiles. This distribution is shown in Figure 13a. For comparison, Figure 13b shows this distribution with a threshold of 28 ppbv, the largest ozone mixing ratio measured during DC-8 boundary layer runs.

There is a large difference between the sonde and the aircraft low ozone measurement distributions, which we attribute to a sampling difference. The sondes were mainly launched in background air, and the planes targeted convection, so the difference is between clear and cloudy air. The DC-8 distribution peaks just below 10 km, while the WB-57 peaks just above, and this is most likely because of the extensive DC-8 in cloud sampling. Evident from

675 both figures is that convective outflow peaks at 10-11 km, a lower altitude in this
676 region than in the Western Pacific. This is consistent with an average cloud top
677 height of 14.2 km derived from the CPL data [*Chang et al., this issue*], also lower
678 than the Western Pacific. Figure 13b also indicates that only 5-10% of air
679 sampled in the maximum outflow region comes directly from the boundary layer
680 without mixing.
681
682 Given the difference between sonde and aircraft measurements of maximum
683 convective outflow, we looked more carefully at the distribution of MHP. The
684 altitude profile of MHP for all TC4 local flights is shown in Figure 14, with the
685 upper tropospheric maximum occurring at 10-11 km, substantiating the aircraft
686 measurements of low ozone. For comparison to fresh convective
687 measurements, the inset (Figure 14b) is a correlation plot of O_3 and MHP
688 measured during the July 24 case study. With the exception of 4-5 data points,
689 all of the elevated MHP (> 300 pptv) occurs at ozone mixing ratios of less than 40
690 ppbv. During this flight the distributions of MHP in the boundary layer ($O_3 \leq 20$
691 ppbv), above the boundary layer in the lower troposphere (2-3 km, $O_3 \sim 30$
692 ppbv), and in the upper tropospheric cloudy measurements are similar. The
693 highest uncertainty of the MHP measurements occurs in humid air, i.e., the
694 marine boundary layer.
695
696 All ozone measured in the upper troposphere is > 30 ppbv. Either the boundary
697 layer air is mixing with mid-tropospheric air (O3 ~ 45 ppbv) during the rapid
698 ascent to 10 -11 km, or the storm is lofting air from 2-3 km. Vertical transport
699 from 2-3 km seems more likely because of the total absence of O3 $\leq$ 20 ppbv. It
700 is unlikely that such rapid mixing would be this efficient.
701
702 We also tested the profile of another low altitude tracer measured from the DC-8
703 and WB-57, in this case the total of measurements of organic bromine species
704 that are produced by marine life in the ocean surface waters. Figure 15a shows
705 a composite of total organic bromine measurements. It is evident from the
706 organic bromine enhancement in the upper troposphere that the altitude of
707 maximum convective outflow occurs at 10-11 km. For comparison, Figure 15b
708 shows the profile of calcium ions measured in bulk aerosol samples as a proxy
709 for dust. In regions impacted by Saharan dust, dust is enhanced in nearby cirrus
710 (Karl Froyd, personal communication). Since the Saharan dust layer is typically
711 found at 2-3 km, this would suggest a significant contribution to convective
712 outflow from this altitude, consistent with what we find most likely using ozone.
713 Very simple mass-balance calculations using ozone, bromine and calcium
714 measurements at 10-11 km suggest that about 50% of the mass in this region of
715 the upper troposphere has been transported upwards from the lower
716 troposphere.
717
718 Summary:
719 The ITCZ is a complex region of small-scale mixing, and typically general
720 circulation models do not perform well in this environment. For understanding

721 convective transport processes, we use ER-2 remote observations to establish
722 context for the DC-8 *in situ* measurements. DC-8 *in situ* measurements in the
723 convectively active upper tropospheric ITCZ region are combined to form a large
724 ensemble. The increase in the number of data points provides statistical tracer
725 relationships that are more robust than in the individual flights. We use tracer
726 gradients and tracer correlations to estimate the boundary layer contribution to
727 the composition of the upper troposphere, to study vertical transport processes in
728 this region of the tropics, and to measure the altitude of greatest convective
729 outflow in tropical maritime convection near Central America.
730
731 We found the troposphere to be well-mixed tropical background air with well-
732 aged pollution and very few distinct plumes of stratospheric or more freshly
733 polluted air. Due to the cloudy nature of this highly convective area, tracer
734 correlations and reactive nitrogen ratios are not effective for studying convective
735 processes. We examine the data from two flight days during which the ER-2 and
736 the DC-8 sampled an actively developing convective system, and a more mature
737 system generating convective outflow. We find that the most robust *in situ* data
738 relationship is an anti-correlation between ozone and the amount of condensed
739 water in cloud.
740
741 When we test a combined data set from DC-8 sampling of the upper troposphere
742 in the “racetracks” patterns, we find that the ozone to CWC inverse relationship is
743 valid, and that the peak of the ozone measurement probability in cloud is 37
744 ppbv. Carbon monoxide measurements imply that there is a net transfer of
745 polluted air from the lower to the upper troposphere. Boundary layer ozone
746 measurements are tightly distributed around 20 – 22 ppbv, lower than the value
747 found in convective clouds by roughly 10-15 ppbv. Measurements of vertical
748 velocity in the active convection and Lagrangian measurements of the ozone
749 production rate from a sonde in convection imply that although the ozone
750 production rate can be large, it is probably not capable of adding the missing 10-
751 15 ppbv during transport. Measurements of methyl hydrogen peroxide do not
752 help to discriminate between transport of air from 2-3 km into the upper
753 troposphere, and boundary layer air that has mixed significantly (50%) during the
754 rapid (~15 minutes) vertical transport to 10-11 km. We note that the sensitivity of
755 MHP measurements in humid air, and therefore the lower troposphere, is
756 relatively poor. However, the speed of vertical transport, the lack of a significant
757 amount of ozone < 28 ppbv and the low variability in ozone mixing ratios
758 measured in active convective outflow suggest that rapid vertical transport of air
759 from 2-3 km is more likely.
760
761 The altitude of maximum convective outflow measured during TC4 is found to be
762 between 10-11 km, characterized by the maximum probability of measuring low
763 ozone, and maximums in the vertical distributions of MHP and total organic
764 bromine. This is significantly lower than predicted by the theoretical model of
765 *Folkins et al.* [2006], which calculates the maximum amount of flux divergence to
766 occur at 12 km, but is consistent with cloud top heights that are also lower (14.2

km, *Chang, this issue*), so that the altitude of maximum convective outflow occurs about 4 km below the cloud tops. It is also lower than indicated by measurements from sondes in the Western Pacific [*Solomon et al.,* 2005]. A rough mass balance calculation of the amount of convective transport using mean ozone, bromine and calcium ions ("dust") suggests that 50% of the air in the upper troposphere below the TTL in this region has been vertically transported there by convection. There does not appear to be a significant amount of undiluted boundary layer air being vertically transported to the upper troposphere, even in very fresh convection

Acknowledgements:
The authors thank NASA Middle Atmosphere and Tropospheric Chemistry Programs for funding and Lenny Pfister for all sorts of meteorological information and consultation. We thank Ru-shan Gao for making ozone measurements from the WB-57, and Holger Voemel for the Alajuela ozonesonde data. Ross Salawitch and Tim Canty provided the plot of total organic bromine, and we are grateful for this. We also thank Mario Rana for DC-8 fast-response tracer lag correlations and Ali Aknan for "Chemical Digital Atlas" plots and calculations of statistical vertical tracer distributions during various tropospheric aircraft field missions (http://www-air.larc.nasa.gov/cgi-bin/datlas). We are grateful to K.A. Masserie and E. Dlugokencky at NOAA CMDL for the Barbados and Bahia methane measurements, and to Pat Minnis and his group for the GOES satellite images.
Keywords:
Convection, tropics, ITCZ, vertical transport, chemical tracers, ozone, condensed cloud water content

Figure Captions:

Figure 1: TC4 local "racetrack" flights: Flight tracks of the NASA DC-8 are shown from above, colored by the amount of *in situ* ozone measured along the way. The flight tracks shown here represent the location of data collected and used in this paper for analysis of the convective outflow region in the upper troposphere. During these flights the DC-8 flight planning featured extensive sampling of active convection or convective outflow in close proximity to the aircraft home base in Alajuela, Costa Rica. Many of the flights show a characteristic "racetrack" pattern, maintained while 2 or 3 planes were stacked vertically.

Figure 2: TC4 Ozone and Carbon Monoxide Median Profiles: This figure shows profiles of the median, the first and third quartile (green boxes), and the 5%-95% distribution (whiskers) of the *in situ* ozone and carbon monoxide measured from the NASA DC-8 by FASTOZ and DACOM during TC4. Data taken between 7S and 17N latitude, and between 70-90W longitudes, is averaged to 30 seconds and binned in 1 km intervals for all the TC4 flights.

Figure 3: Profiles of the median ozone concentration calculated using 30 second averaged data sampled between 7S and 17 N latitude during various aircraft field missions over the tropical Pacific and Western Atlantic oceans. The data is binned at 1 km vertical resolution, and extends over the same latitudinal range of the tropics as does the TC4 mission. The historical data is shown as context for comparison with the TC4 data, which is shown in green.

Figure 4: A plot of ozone concentrations are shown versus methane measured using the DACOM instrument. They are uncorrelated, and this reflects how well-mixed the air is in the TC4 study area of active tropical convection. NOAA CMDL measurements of methane from the closest Southern and Northern Hemispheric surface sampling stations is shown for comparison with the aircraft measurements.

Figure 5: This figure is a composite of images from the ER-2 and DC-8 on July 24, 2007, when the DC-8 flew through a developing convective system and was hit by lightning. Panel a is a GOES visible image showing clouds during the high-altitude portion of the DC-8 flight through active convection. The DC-8 (blue) and ER-2 (red) flight tracks are superimposed on this image, which was provided by Patrick Minnis, NASA Langley. Panel b is a 3-dimensional view of the CPL lidar image, showing the cloud tops and the DC-8 track (colored by ozone) through the storm. Panel C shows the time series of condensed cloud water content, ozone, carbon monoxide and altitude from the DC-8 during the flight. Panel D is an expanded view of ozone and condensed cloud water content measured by the CVI and 2DS instruments in the upper troposphere in actively developing convection. The large spikes in CWC were measured by the 2DS probe during saturation of the CVI instrument in the convective cores.

Figure 6: Panel a of his figure shows a photograph from the DC-8 forward-looking video that shows the vigorous convection sampled on July 24, 2007. The second panel shows data from 11 km in the location of the green arrow in the video still. The vertical velocity was measured *in situ* by the MMS on the DC-8, in red, and ice water content (black) and particle density (blue) were measured by the 2D-S cloud probe. The peak vertical velocity of 20 m/s occurs with the large ice water concentration of 2.4 g/m3, indicated on the plot.

Figure 7: Carbon monoxide, CO (red diamonds in ppb), ozone, O_3 (black + in ppb), methyl-hydrogen peroxide, CH_3OOH (green triangles in pptv/10), and peroxy-nitric acid, HO_2NO_2 (blue X in pptv) during racetrack portion of the 24 July flight. Horizontal lines shown at times 5.37-5.39e4 show averages during preceding boundary layer leg and standard error of the mean as a vertical line through the center.

Figure 8: Map (degrees latitude and longitude) of the racetrack portion of the flight (5.36-5.65e4 GMT sec). Red triangles: air mass with tracer-tracer correlations distinctly different from the boundary layer (5.475e4-5.52e4 and 5.61e4-5.65e4 GMT sec); Blue stars: elsewhere (tracer-tracer correlations similar to boundary layer) and $O_3 < 40$ ppb; Green: elsewhere and $O_3 > 50$ ppb. Boxes show approximate nadir footprints of OMI (smallest, turquoise), SCIAMACHY (medium, pink), and GOME2 (largest, orange).

Figure 9: Panel “a” shows OMI/MLS tropospheric ozone mean volume mixing ratio (units ppbv) measured during the 18:30 Z overpass of the AURA satellite on July 24, 2007. The DC-8 flight path for this day is shown, with most aircraft sampling performed when the DC-8 was circling near 225 hPa inside the active convective system. Panel b shows the corresponding IR color-enhanced GOES image, which can be compared to the earlier image shown in Figure 5. A loop of GOES images between these two clearly shows the convective outflow streaming off to the southwest, coincident with OMI measurements of low ozone (blue).

Figure 10: Several plots of ozone, CO, condensed cloud water and cloud images are shown here from the August 5th flights of the DC-8 and ER-2. A movie showing the CALIOP, CPL and DC-8 cloud data together on this day in 3-dimensions is available at *add link. Figure 10a is a 3-dimensional still image of the entire DC-8 and ER-2 flights. The CPL shows the location of the cirrus anvils sampled, with cloud tops at 14 km, 3-5 km above the DC-8. The Dc-8 flight track is colored by *in situ* ozone. Overlain above this image is a repeated DC-8 flight track, colored by carbon monoxide. Figure 10b shows the time series of CO (pink) ozone (black) and CWC (blue) from the DC-8 during the racetracks. The trace shows spikes of high ozone and lower CO on the dry side of the racetrack, outside of the cirrus anvil. Figure 10c is a correlation plot of ozone and condensed cloud water, with very heavy clouds (CWC > 0.1 g/m3) colored in red.

Figure 11: A plot of ozone concentration in ppbv on the y-axis, versus condensed cloud water content measured by the CVI instrument in the upper troposphere during the "racetrack" flights is shown here. Points with condensed cloud water content greater than 0.2 g/m^3 represent data taken in heavy clouds, and is colored in red. A smaller threshold of 0.01 was chosen to represent data taken "in cloud" and "out of cloud".

Figure 12: Shown in Figure 12a are normalized probability distribution histograms for ozone data measured during upper tropospheric "racetracks" when the DC-8 was in a cloud (blue) and not in a cloud (red). A threshold of 0.01 g/m3 of equivalent liquid condensed cloud water was chosen to divide the data set. The choice of this threshold is described in the text. Normalized probability distributions for carbon monoxide inside (blue) and outside (red) of clouds are shown in Figure 12b, similar to Figure 12a for ozone.

Figure 13: This figure shows a profile of the probability of occurrence of low ozone in 500 meter vertical bins for the WB-57 and the DC-8 TC4 ozone data from local flights, and for the Alajuela and Panama sonde measurements. Panel "a" shows the probability of measuring $O_3 < 44$ ppbv, a threshold derived from the probability distribution shown in Figure 12 to include the "in cloud" low ozone peak. For comparison, panel "b" shows $P(O_3 < 28$ ppbv), which includes all measured boundary layer values, but less than 25% of ozone measured at 2 km and above.

Figure 14: Altitude profile of MHP mixing ratio as measured from DC8 in all local flights during TC4. Gray crosses are individual (1 s) points. Red trace is the median of 1-km altitude bins; whiskers show the first and third quartiles for these bins. For comparison, the inset is a correlation plot of O_3 and MHP from the July 24 flight n very fresh, developing convection.

Figure 15: Panel "a" of this figure is the profile of total organic bromine measured by gas chromatography performed on whole air samples taken from the NASA ER-2 and the DC-8 during the TC4 field campaign. Total organic bromine is shown here as a tracer for boundary later air. Panel "b" shows an aggregate profile of calcium ion concentrations taken from all available bulk air samples taken during the TC4 local flights. Calcium is used as a proxy for Saharan dust.

924 References:
925
926 Bertram, T., et. al., Direct measurements of the convective recycling of the upper troposphere,
927 *Science*, 315, 816-820, doi:10.1126/science.1134548, 2007.
928
929 Bucsela, E., et. al. (2010), Lightening-generated NO_x seen by OMI during NASA's TC4
930 experiment, *J. Geophys. Res.,* this issue.
931
932 Burrows, J.P., E. Hölzle, A.P.H. Goede, H. Visser, W. Fricke, SCIAMACHY- Scanning Imaging
933 Absorption Spectrometer for Atmospheric Chartography, *Acta Astronautica*, 35, 445, 1995.
934
935 Callies, J., E. Corpaccioli, M. Eisinger, A. Hahne and A. Lefebvre, GOME-2 - MetOp's Second
936 Generation Sensor for Operational Ozone Monitoring, European Space Agency Bull., 102,
937 2000.
938
939 Dibb, J., et al., 2003. Aerosol chemical composition in Asian continental outflow during TRACE-P:
940 comparison to PEMWest B. *J. Geophys. Res*. 108 (D21), 8815.
941
942 Folkins, I., P. Bernath, C. Boone, L.J. Donner, A. Eldering, G. Lesins, R.V. Martin, B.-M.
943 Sinnhuber, and K. Walker (2006), Testing convective parameterizations with tropical
944 measurements of HNO_3, CO, H2O, and O_3: Implications for the water vapor budget, *J.*
945 *Geophys. Res*., Vol. 111, D23304, doi:10.1029/2006JD007325.
946
947 Folkins, I., P. Bernath, C. Boone, K. Walker, A.M. Thompson, and J.C. Witte, The seasonal
948 cycles of O_3, CO and convective outflow at the tropical tropopause, *Geophys. Res. Let*., 33,
949 L16802, doi:10.1029/2006GL026602.
950
951 Folkins, I., C. Braun, A.M. Thompson, J.C. Witte (2002), Tropical ozone as an indicator of deep
952 convective outflow, *J. Geophys. Res*., 107, D13, doi: 10.1029/2001JD001178.
953
954 Folkins, I., M. Lowenstein, J. Podolske, S.J. Oltmans, and M. Profitt (1999), A barrier to vertical
955 mixing at 14 km in the tropics: Evidence from ozonesondes and aircraft measurements, *J.*
956 *Geophys. Res*., Vol. 104(D18), 22095-22102.
957
958 Froidevaux L, Y. B. Jiang, A. Lambert, et al. (2008), Validation of Aura Microwave Limb Sounder
959 stratospheric ozone measurements, J. Geophys. Res., 113, D16, D16S41,
960 doi:10.1029/2007JD008771.
961
962 Gregory, G.L., C.H. Hudgins, J. Ritter and M. Lawrence (1987), In situ ozone instrumentation for
963 10-Hz measurements: Development and evaluation, Proceedings of sixth symposium on
964 Meteorological Observations and Instrumentation, New Orleans, LA, Jan 12-16, 136-139.
965
966 Gregory, G., et. al. (1988), Boundary layer ozone: An Airborne Survey Above the Amazon Basin,
967 *J.Geophys. Res.,* Vol 93(D2), 1452-1468.
968
969 Heymsfield, G.M., L. Tian, A.J. Heymsfield, L. Li, and S. Guimond (2009), Characteristics of deep
970 tropical and subtropical convection from nadir-viewing high-altitude airborne Doppler radar, *J.*
971 *Atmos. Sci*., in press.
972
973 Hlavka, D., L. Tian, W. Hart, L. Li, M. McGill, and G. Heymsfield (2010), Vertical cloud climatology
974 during TC4 derived from high-altitude aircraft merged lidar and radar, *J. Geophys. Res.,* this
975 issue.
976
977 Joiner J., and A. P. Vasilkov (2006), First results from the OMI rotational Raman scattering cloud
978 pressure algorithm, 44, 5, 1272-1282.

Joiner, J., M. R. Schoeberl, A. P. Vasilkov, et al. (2009), Accurate satellite-derived estimates of the tropospheric ozone impact on the global radiation budget, Atmos. Chem. Phys., 9, 13, 4447-4465.

Kley, D., P.J. Crutzen, H.G.J. Smit, H. Vomel, S.J. Oltmans, H.R. Grassi, and V. Ramanathan (1996), Observations of near-zero ozone concentrations over the convective Pacific – effects on air chemistry, *Science*, 274, 230-233.

Lawson, R.P., E.J. Jenson, B. Baker, and Q. Mo (2010), Microphysical and radiative properties of tropical clouds investigated in TC4 and NAMMA, *J. Geophys. Res.*, this issue.

Lawson, R. P., D. O'Connor, P. Zmarzly, K. Weaver, B. A. Baker, Q. Mo, and H. Jonsson, 2006: The 2D-S (Stereo) Probe: Design and Preliminary Tests of a New Airborne, High Speed, High-Resolution Particle Imaging Probe. *J. of Atmos. and Oceanic Technol.*: Vol. 23., No. 11, pp. 1462-1477.

Levelt, P. F., et al., The Ozone Monitoring Instrument, IEEE Trans. on Geosci. and Rem. Sens., 44, 1093-1101, 2006.

McGill, M.J., D.L. Hlavka, W.D. Hart, J.D. Spinhirne, V.S. Scott, and B. Schmid, "The Cloud Physics Lidar: Instrument description and initial measurement results", *Applied Optics,* 41, pg. 3725-3734, June 2002.

Minnis, P., L. Nguyen, R. Palikonda, J. K. Ayers, R. F. Arduini, F.-L. Chang, T. L. Chee, D. R. Doelling, P. W. Heck, M. M. Khaiyer, M. L. Nordeen, W. L. Smith, Jr., D. A. Spangenberg, C. R. Yost, P. Yang, and Y. Xie, (2010) Cloud properties determined from GOES and MODIS data during TC4, *J. Geophys. Res.*, this issue.

Morris, G.A., et. al. (2010), Observations of ozone production in a dissipating convective cell during TC4, *J. Geophys. Res.*, this issue.

Oltman, S.J., et. al., Ozone in the Pacific tropical troposphere from ozonesonde observations, *J. Geophys. Res.*, 106, 32503-32526, 2001.

Pearson R.W. and D.H. Stedman (1980), Instrumentation for fast response ozone measurements from aircraft*, Atmos Tech*, 12.

Pfister, L., H.B. Selkirk, D. O'C. Starr, P.A. Newman, and K.H. Rosenlof (2010), A meteorological overview of the TC4 mission, *J. Geophys. Res.*, this issue.

Ridley, B. A., M. A. Avery, J. V. Plant, S. A. Vay, D. D. Montzka, A. J. Weinheimer, D. J. Knapp, J. E. Dye, E. C. Richard, (2006), Sampling of Chemical Consituents in Electrically Active Convective Systems: Results and Cautions, *J. Atmos. Chem.*, 10.1007/s10874-005-9007-5.

Sachse, G., G. Hill, L. Wade, and M. Perry (1987), Fast-Response, High-Precision Carbon Monoxide Sensor Using a Tunable Diode Laser Absorption Technique, *J. Geophys. Res.*, 92(D2), 2071-2081.

Scheuer, E., J.E. Dibb, C. Twohy, D.C. Rogers, A.J. Heymsfield, and A. Bansomer (2010), Evidence of nitric acid uptake in warm cirrus clouds during the NASA TC4 campaign, *J. Geophys. Res.*, this issue.

Schoeberl, M. R., J. R. Ziemke, B. Bojkov, et al. (2007), A trajectory-based estimate of the tropospheric ozone column using the residual method, J. Geophys. Res., 112, D24S49, doi:10.1029/2007JD008773.

Scott, S.G., T.P. Bui, K. R. Chan, and S. W. Bowen (1990), The meteorological measurement system on the NASA ER-2 aircraft, *J. Atmos. Ocean. Tech*., 7, 525-540.

Selkirk, H.B., H Vomel, J.Valverde, and L. Pfister (2010), The detailed structure of the tropical upper atmosphere as revealed by balloonsonde observations of water vapor, ozone, temperature and winds during the NASA TCSP and TC4 campaigns, *J. Geophys. Res*., this issue.

Solomon, S., D.W.J. Thompson, R.W. Portmann, S.J. Oltmans, and A.M. Thompson (2005), On the distribution and variability of ozone in the tropical upper troposphere: Implications for tropical deep convection and chemical-dynamical coupling, *Geophys. Res. Let*., 32, L23813, doi:10.1029/2005GL024323.

Spencer, K.M., D. C. McCabe, J. D. Crounse, J. R. Olson, J. H. Crawford, A. J. Weinheimer, D. J. Knapp, D. D. Montzka, C. A. Cantrell, R. S. Hornbrook, R. L. Mauldin III, and P. O. Wennberg (2009), Inferring ozone production in an urban atmosphere using measurements of peroxynitric acid, *Atmos. Chem. Phys*., 9, 3697-3707.

Thompson, A.M. et. al. (2010), Convective and wave signatures in ozone profiles over the equatorial Americas: Views from TC4 (2007) and SHADOZ, *J. Geophys. Res*., this issue.

Thompson, A.M., J.E. Yorks, S.K. Miller, J.C. Witte, K.M. Dougherty, G.A. Morris, D. Baumgerdner, L. Ladibno, and B. Rappenglueck, Tropospheric ozone sources and wave activity over Mexico City and Houston during Milagro/Intercontinental Transport Experiment (INTEXB) Ozonesonde Network Study, 2006 (IONS-06), *Atmos. Chem. Phys*., 8, 5113-5125, 2008.

Toon, O.B., D. O'C. Starr, E. Jensen, P. Newman, S. Platnik, M. Schoeberl, P. Wennberg, S. Wofsy, M. Kurylo, H. Maring, K. Jucks, M. Craig, M. Vasquez, et. al., Planning and overview of the Tropical Composition, Cloud and Climate Coupling Experiment, *J. Geophys. Res*., this issue.

Twohy, C.H., Schanot, A.J. and W.A. Cooper, 1997: Measurement of condensed water content in liquid and ice clouds using an airborne counterflow virtual impactor, *J. Atmos. Oceanic Technol*., **14**, 197-202.

Winker, D. M., W. H. Hunt, and M. J. McGill, (2007), Initial performance assessment of CALIOP, *Geophys. Res. Lett*., 34, L19803, doi:10.1029/2007GL030135.

Ziemke, J. R., J. Joiner, S. Chandra, P. K. Bhartia, A. Vasilkov, D. P. Haffner, K. Yang, M. R. Schoeberl, L. Froidevaux, and P. F. Levelt (2009), Ozone mixing ratios inside tropical deep convective clouds from OMI satellite measurements, *Atm. Chem. Phys*., 9, 573-583.

Ziemke, J. R., S. Chandra, and P. K. Bhartia (2001), "Cloud slicing": A new technique to derive upper tropospheric ozone from satellite measurements, J. Geophys. Res., 106, 9853-9867.

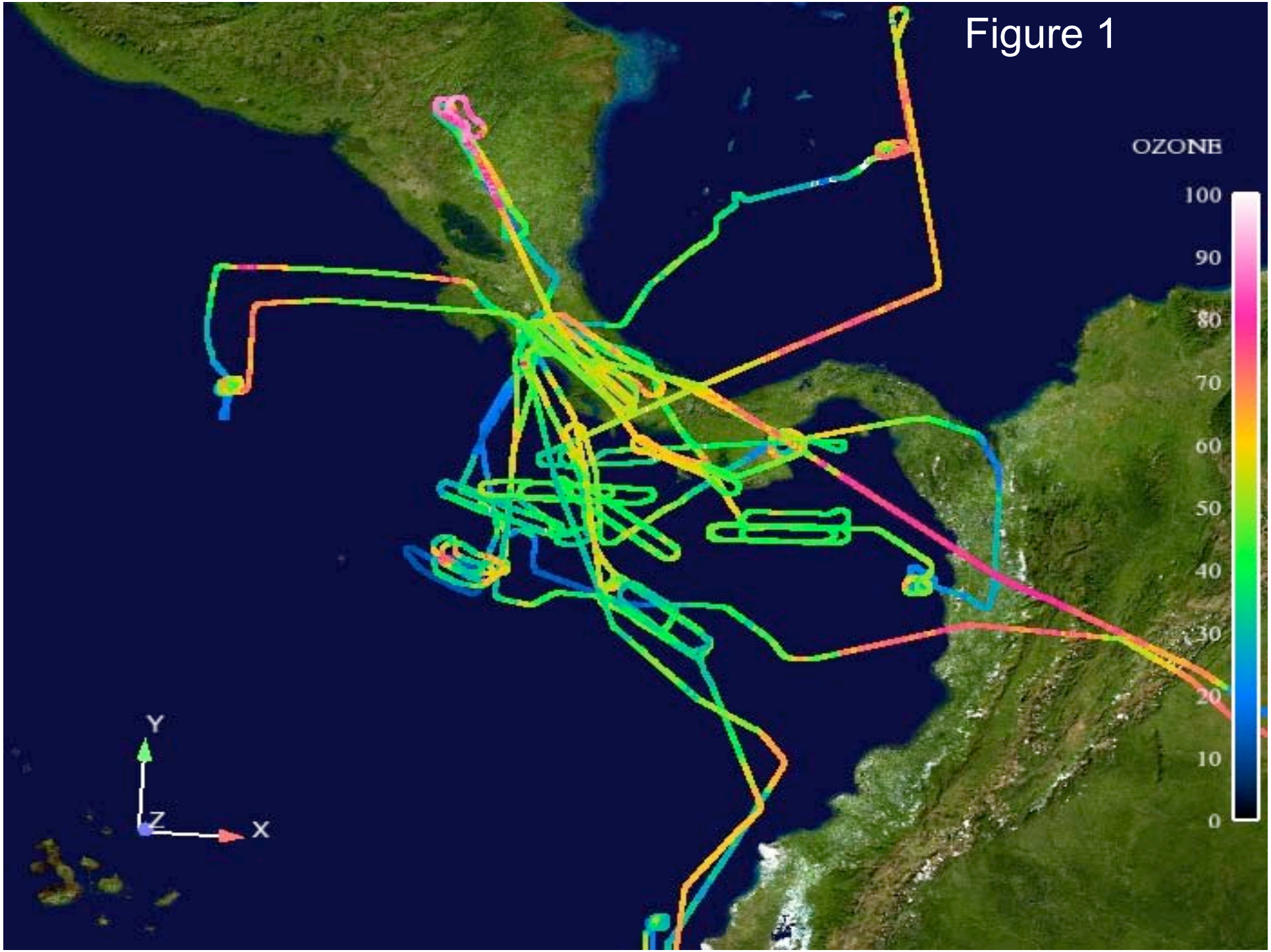
Figure 1
OZONE
100
90
80
70
60
50
40
30
20
10
0
Y
Z
X

Figure 2

Overview: TC4 Ozone and CO Median Profiles

7S - 17N, 270W - 290W

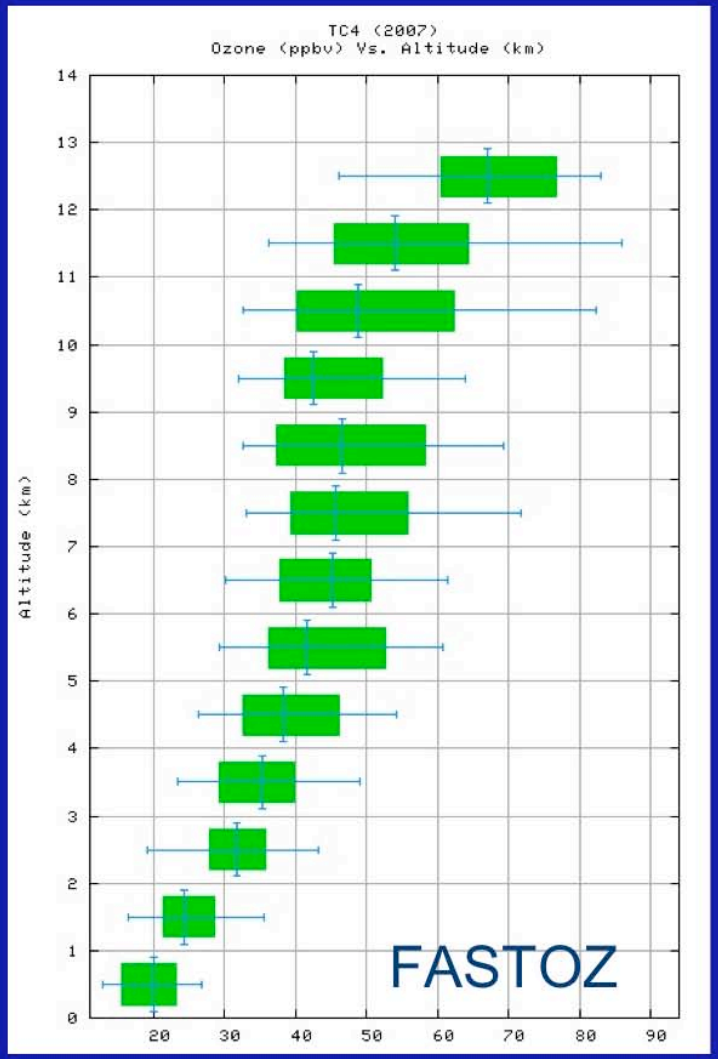

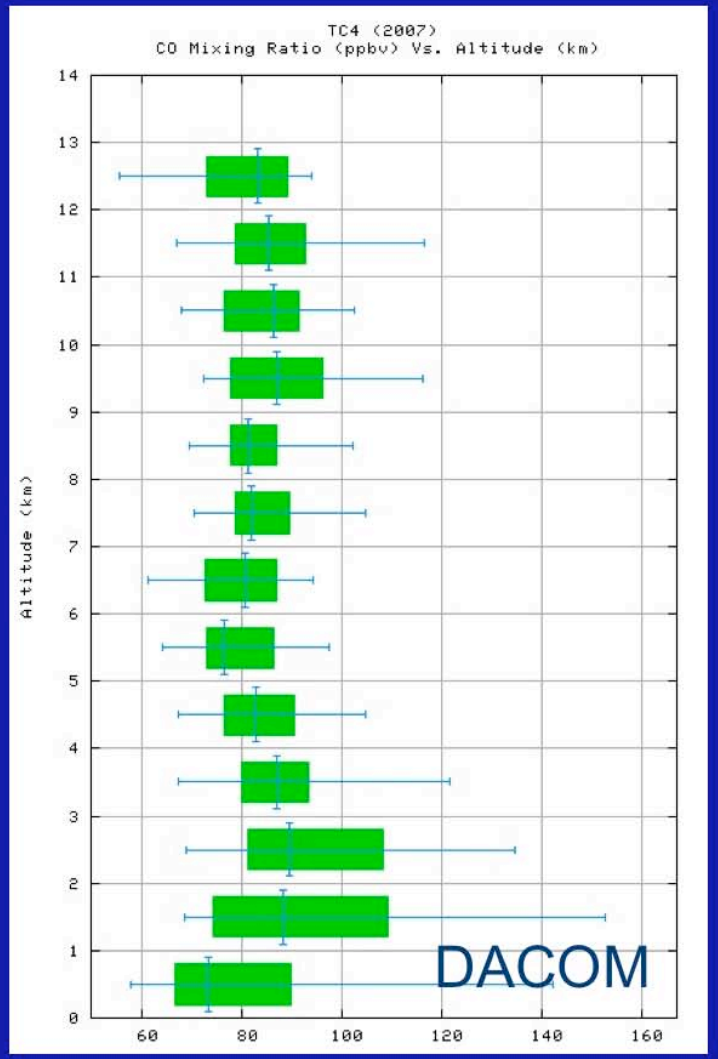

Figure 3

Ozone Medians from Pacific Missions

Data Range: 7S - 17N

ABLE (Amazon) 1980's, PEM Tropics 1990's

All Missions were Neutral or Cold Phase ENSO (!)

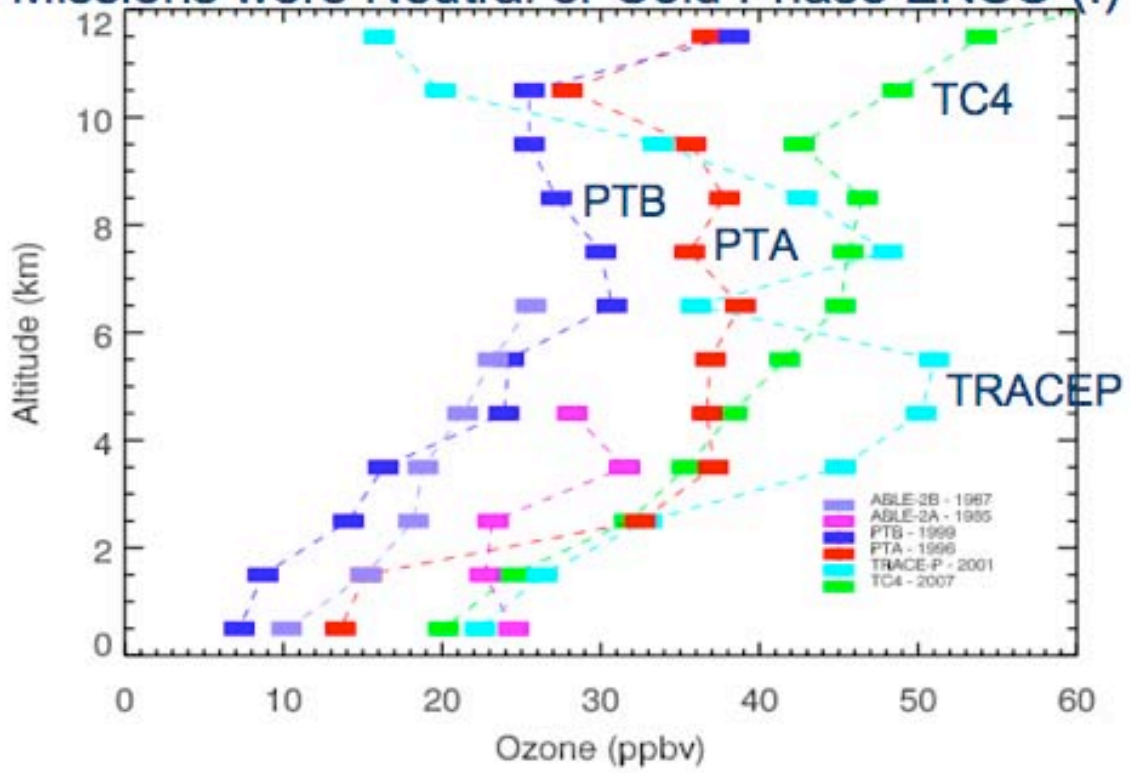

Ozone Medians calculated using the Langley Digital Chemical Atlas

Figure 4

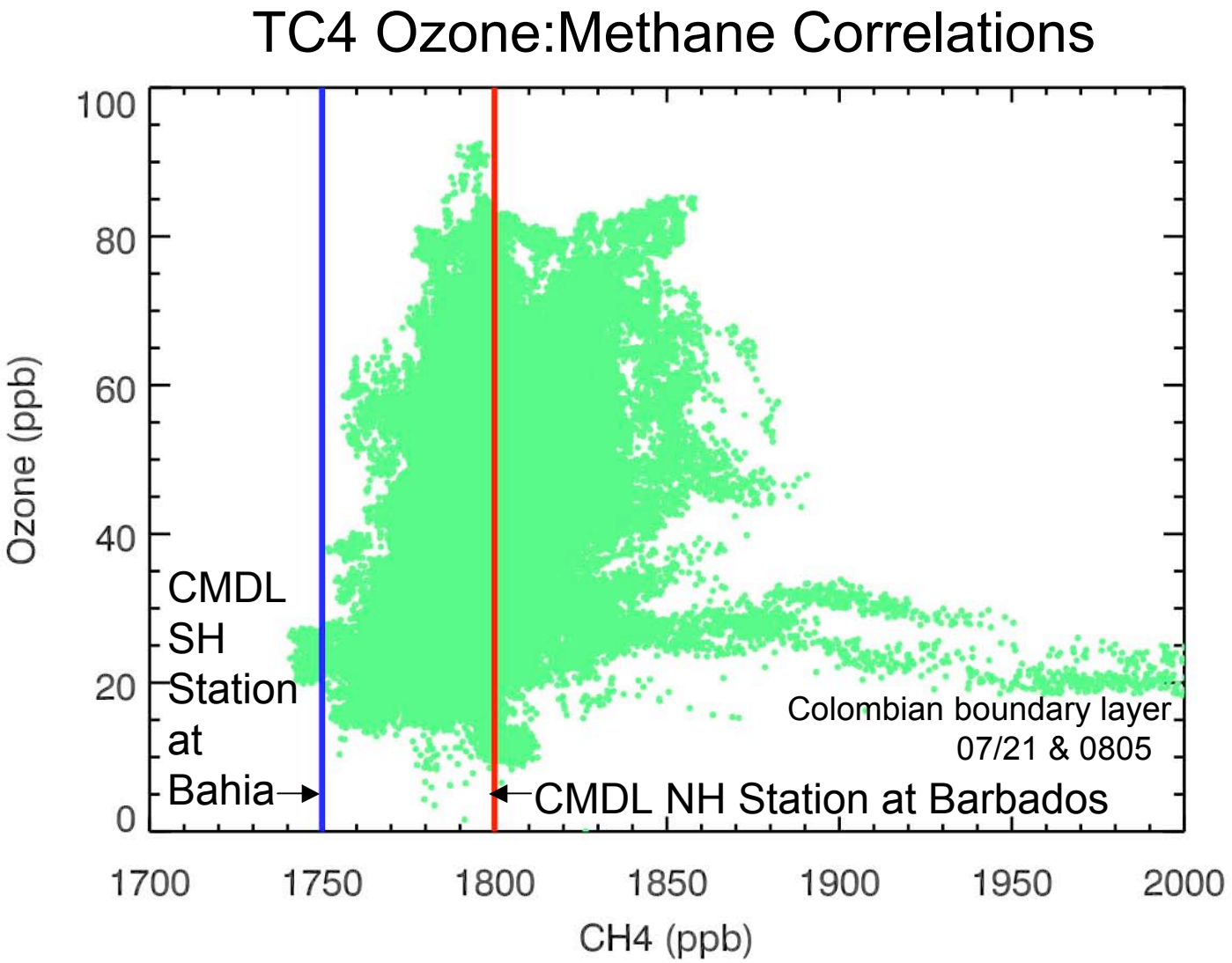

NOAA/CMDL methane data: K. A. Maserie and E. Dlugakencky

July 24 - DC-8 sampling Inside Active Convection

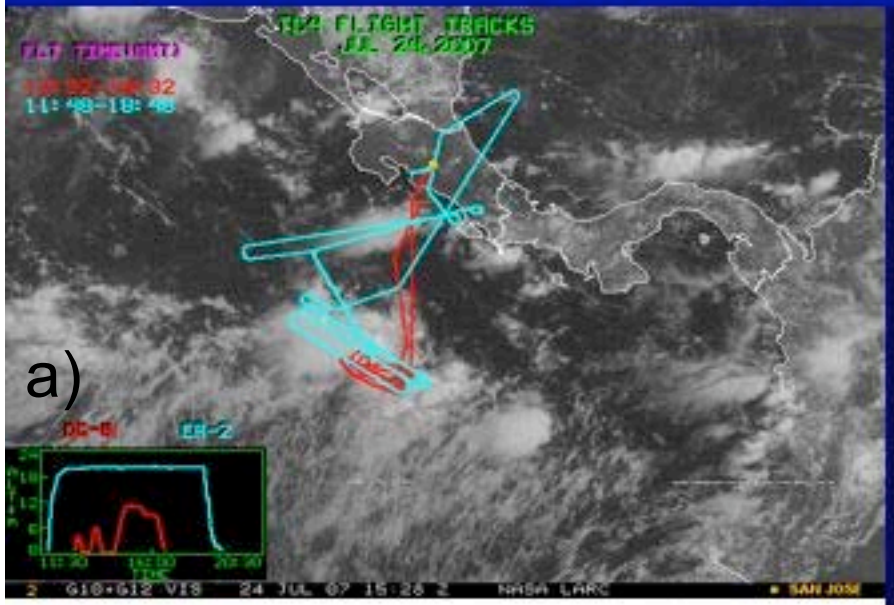

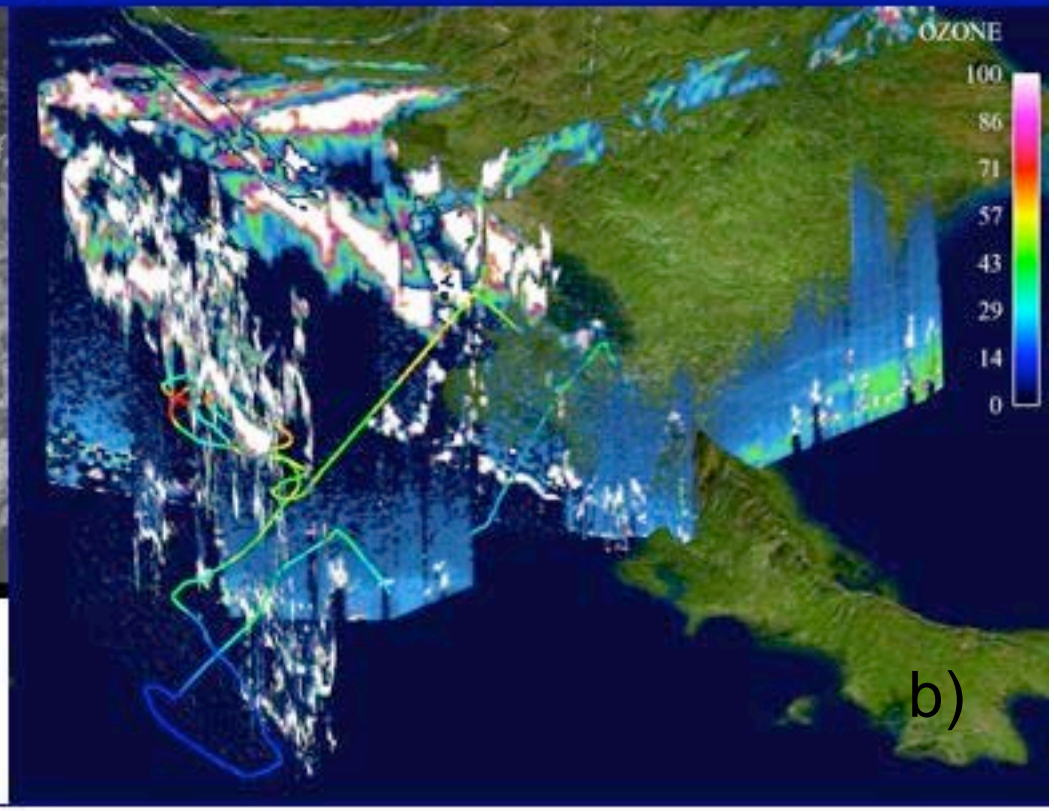

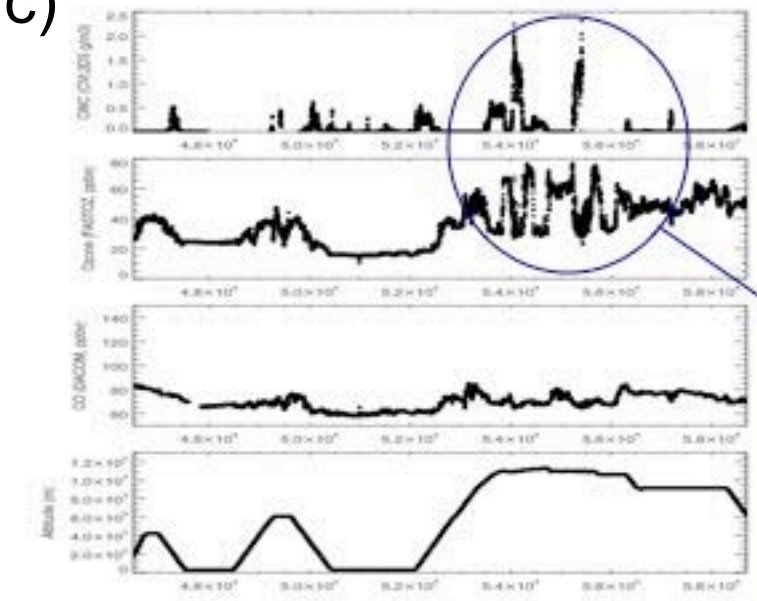

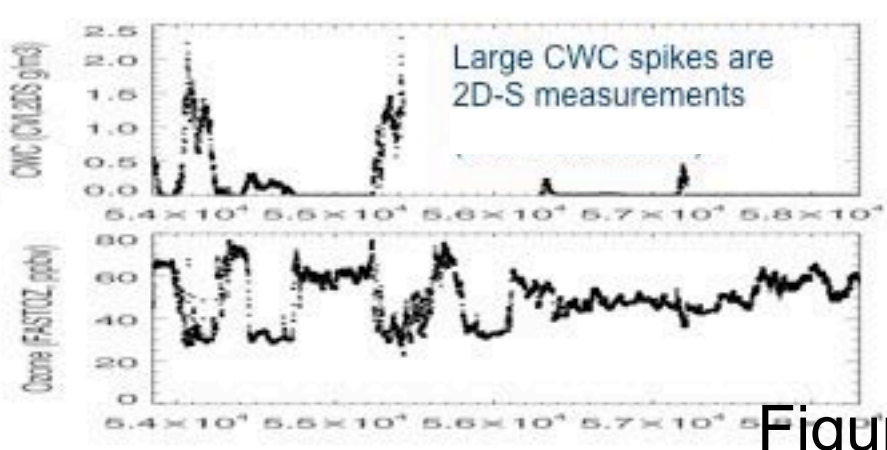

Figure 5

Strong Convection on
July 24, 2007 During TC4

Figure 6

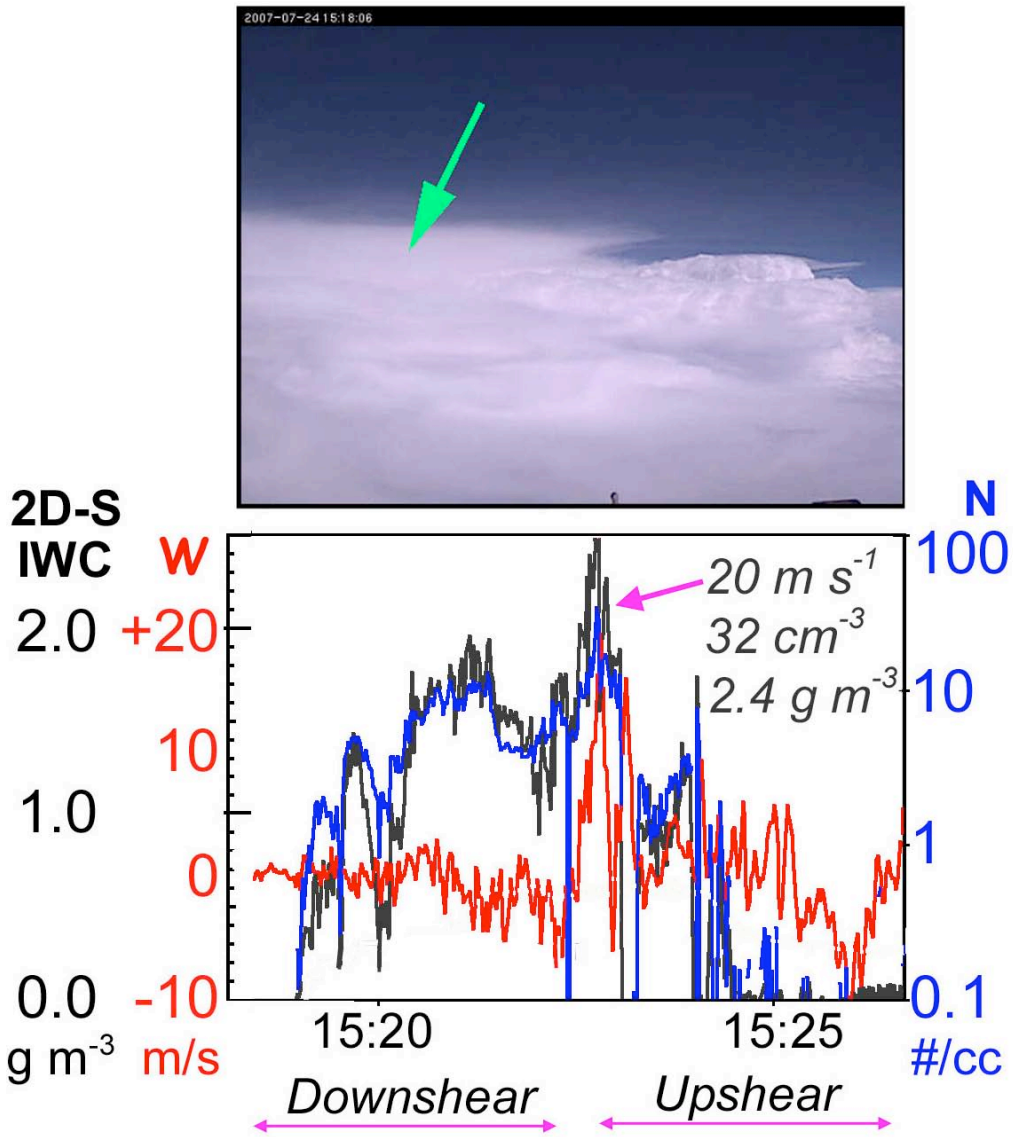

Figure 7

Upper Tropospheric Tracer Time Series
in Fresh Convection

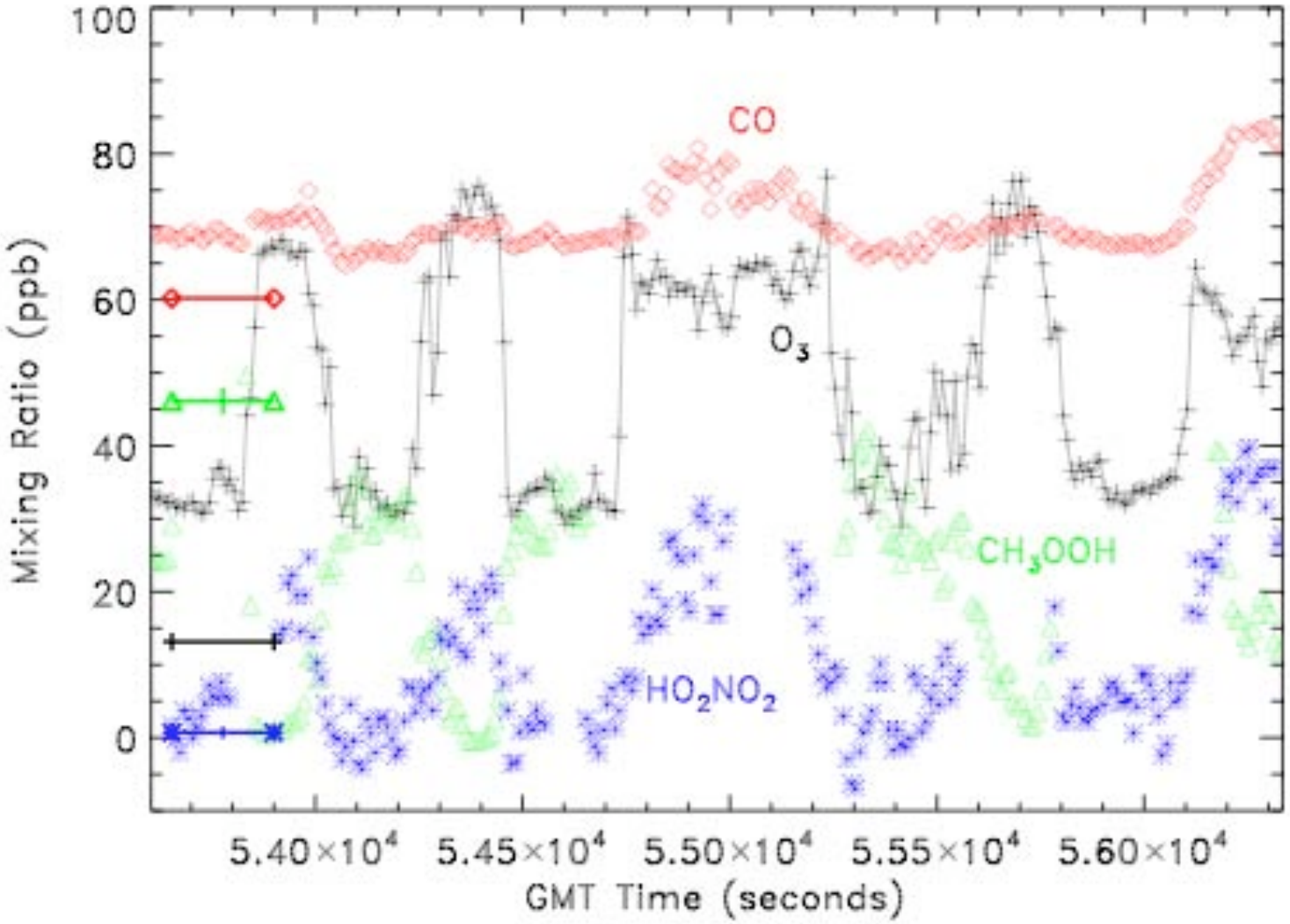

Figure 8

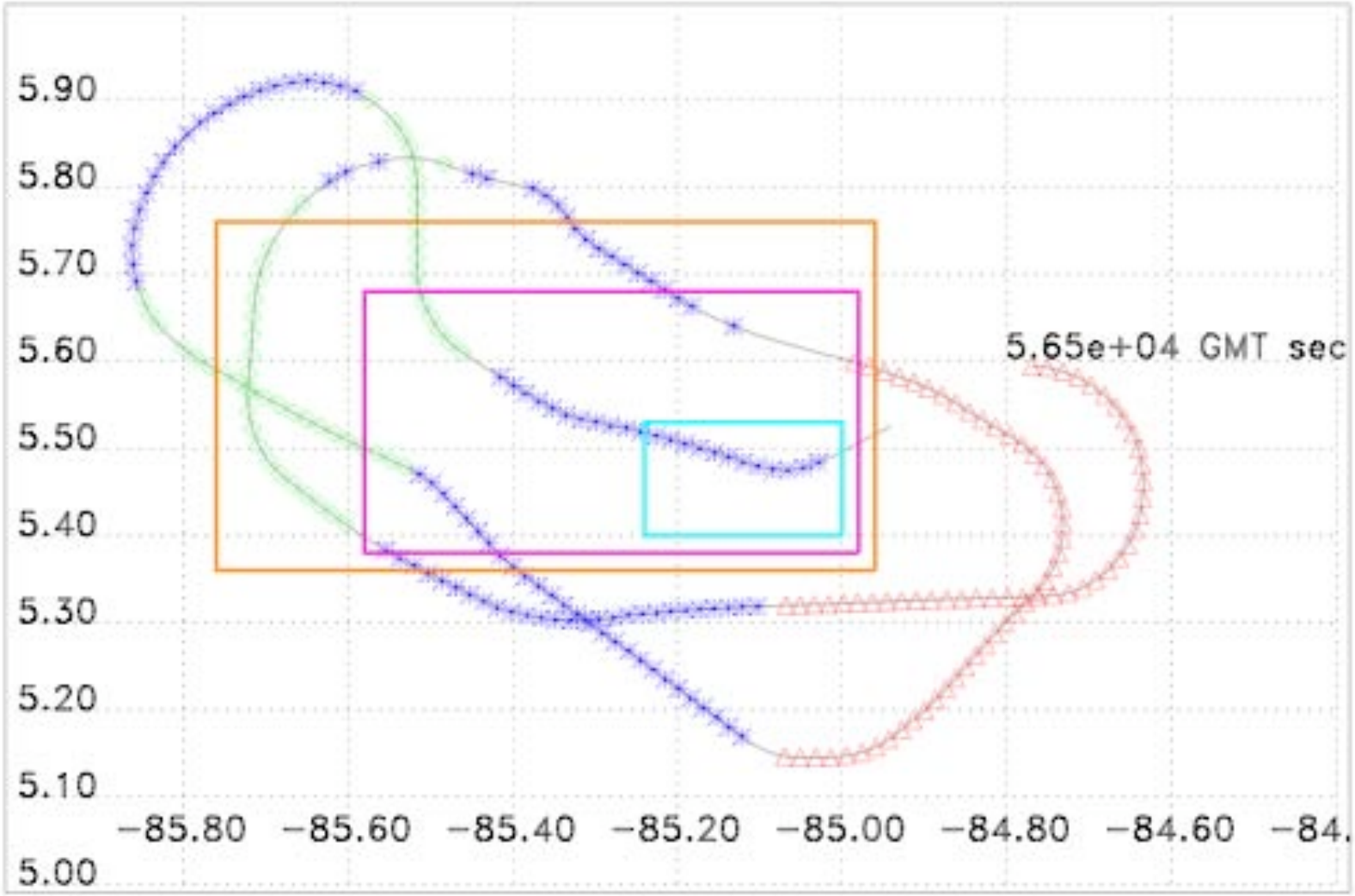
5.90
5.80
5.70
5.60
5.50
5.40
5.30
5.20
5.10
5.00
−85.80
−85.60
−85.40
−85.20
−85.00
−84.80
−84.60
−84.
5.65e+04 GMT sec

Figure 9

OMI Mean Tropospheric Ozone and GOES IR Image

TC4 July 24 Overpass, 18:30 Z

a) OMTO3 Mean Tropo O3 (ppbv) All Scenes 24Jul07

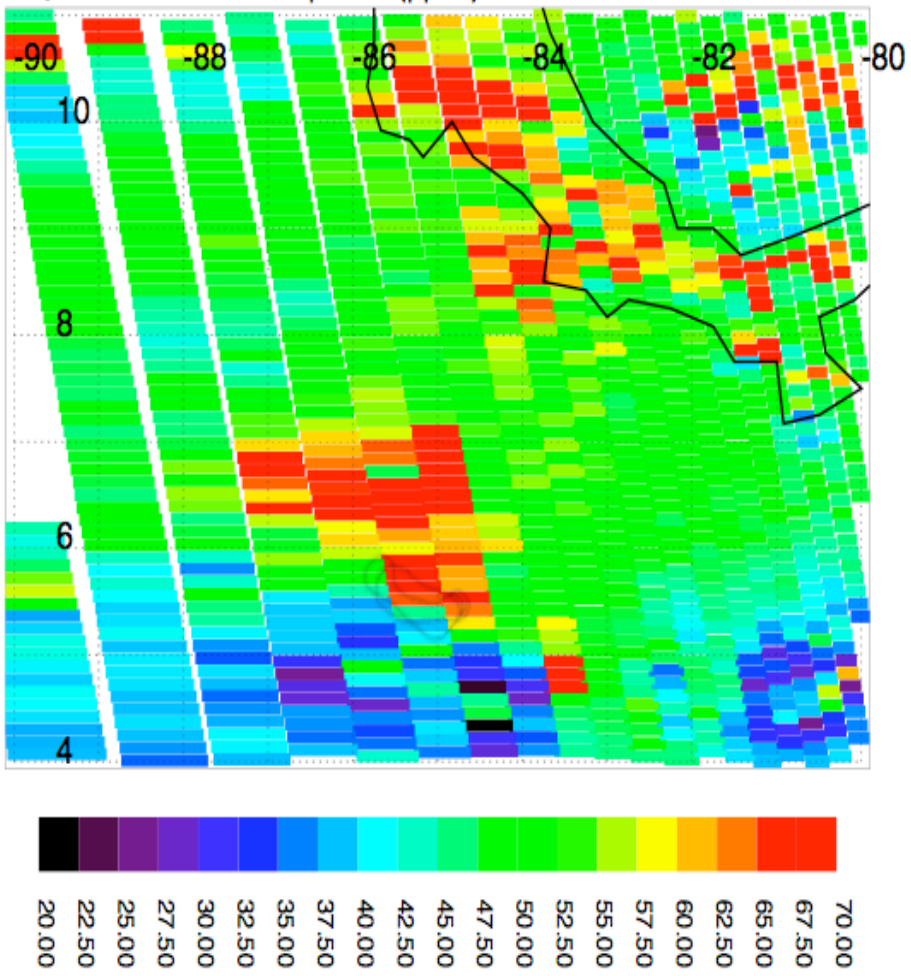

b) GOES IR 4km Color Image

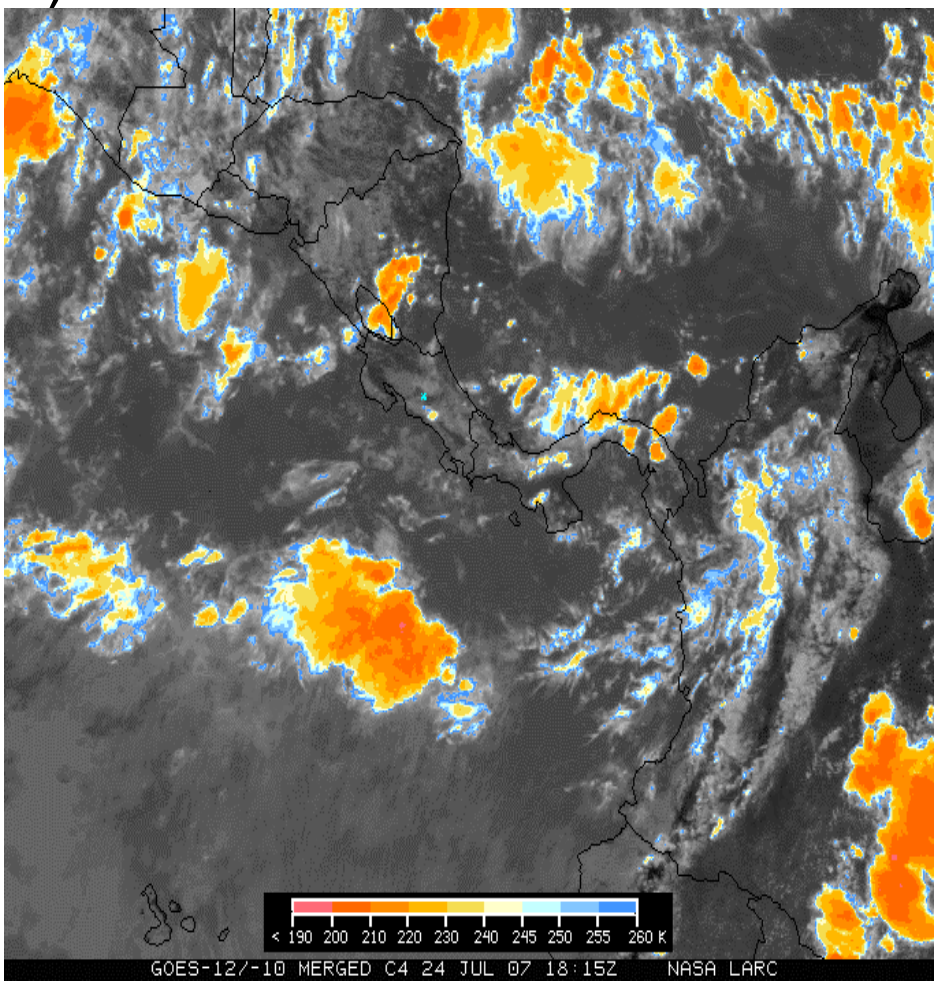

Figure 10

August 5: Close-Up of Convective Outflow

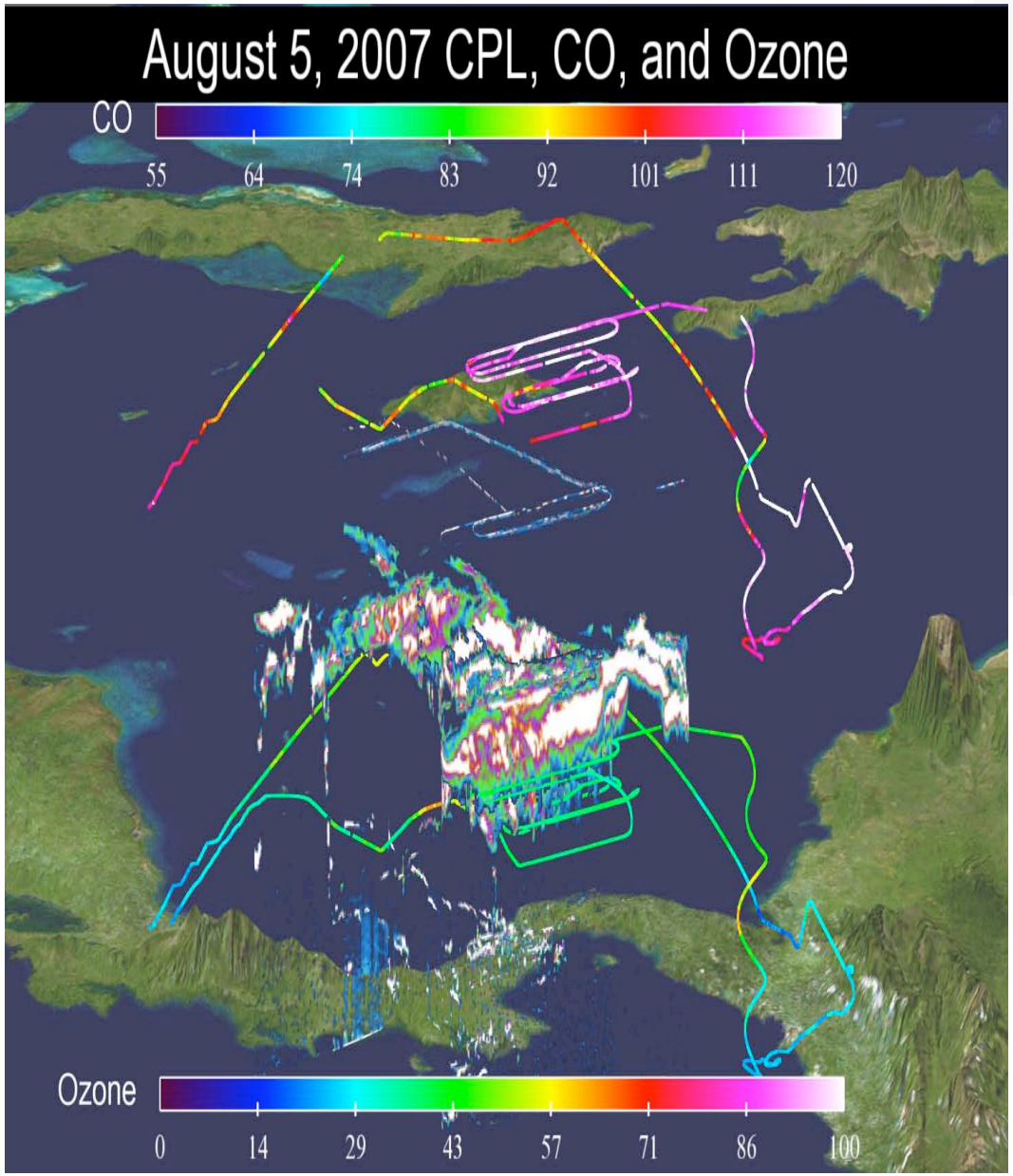

Time Series of CO, Ozone and CWC

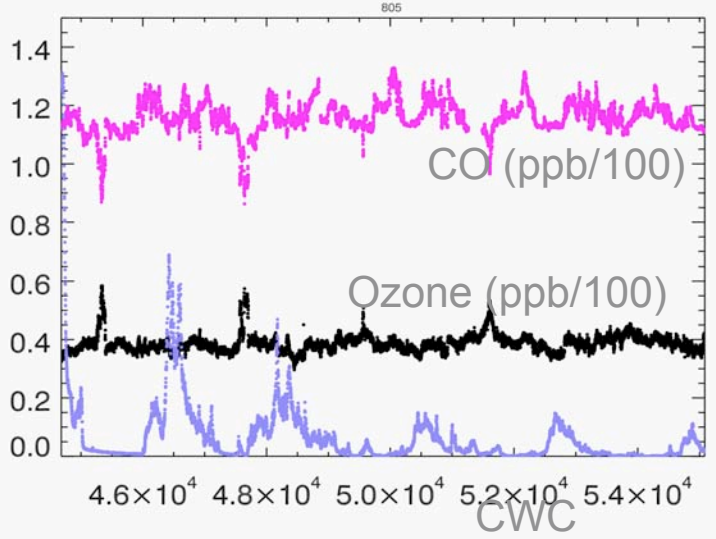

Ozone (ppb) vs CWC (g/m^3)

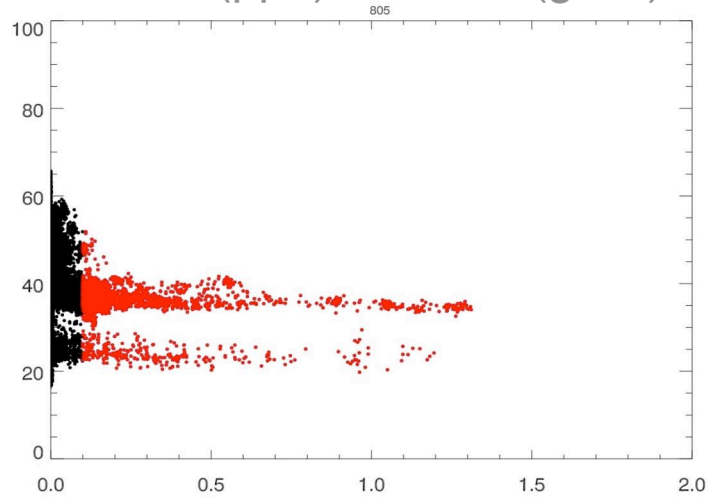

Figure 11

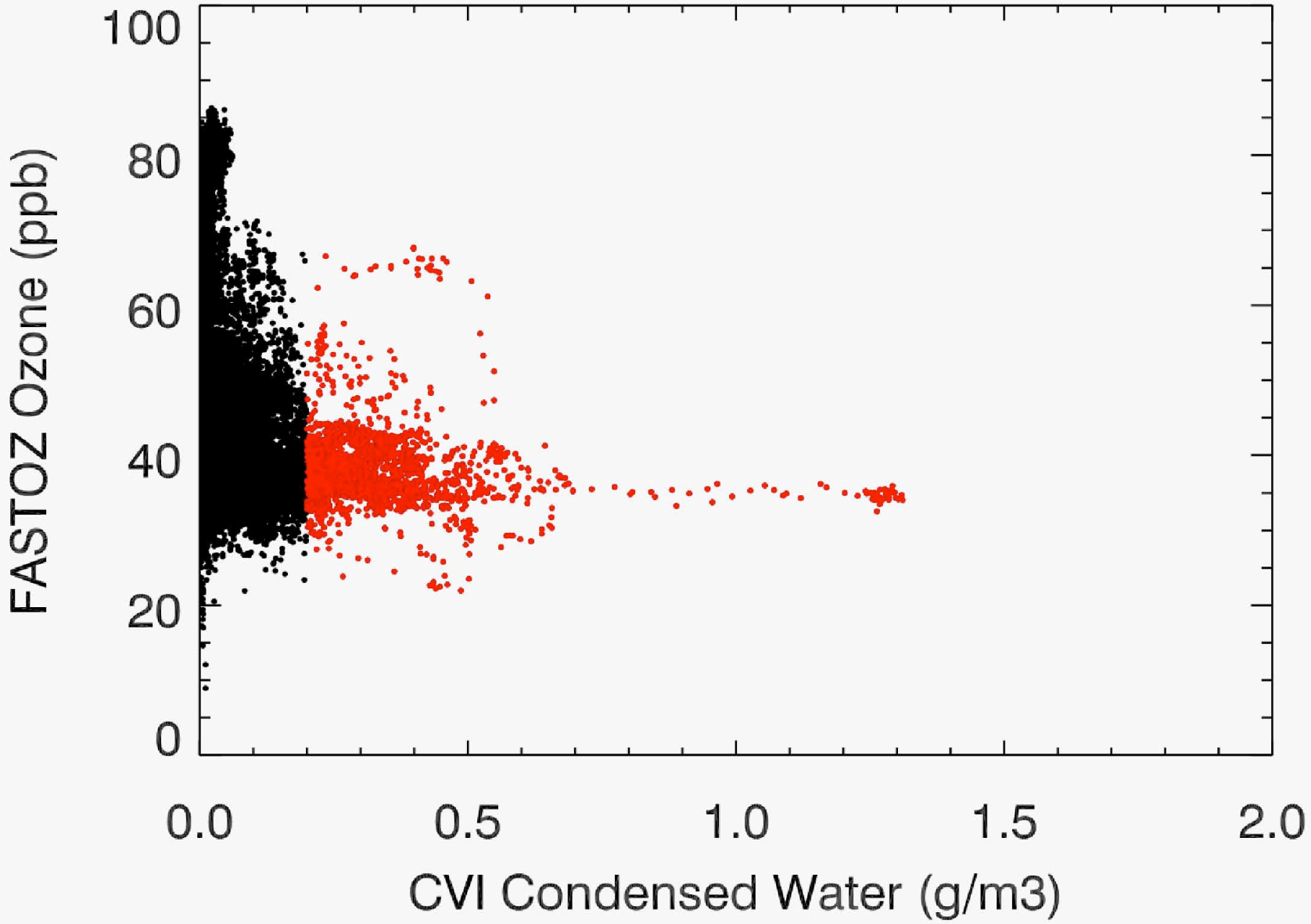
100
80
60
40
20
0
FASTOZ Ozone (ppb)
0.0
0.5
1.0
1.5
2.0
CVI Condensed Water (g/m3)

Figure 12

Probability Histograms of Ozone and Carbon Monoxide

In Clouds and Outside of Clouds

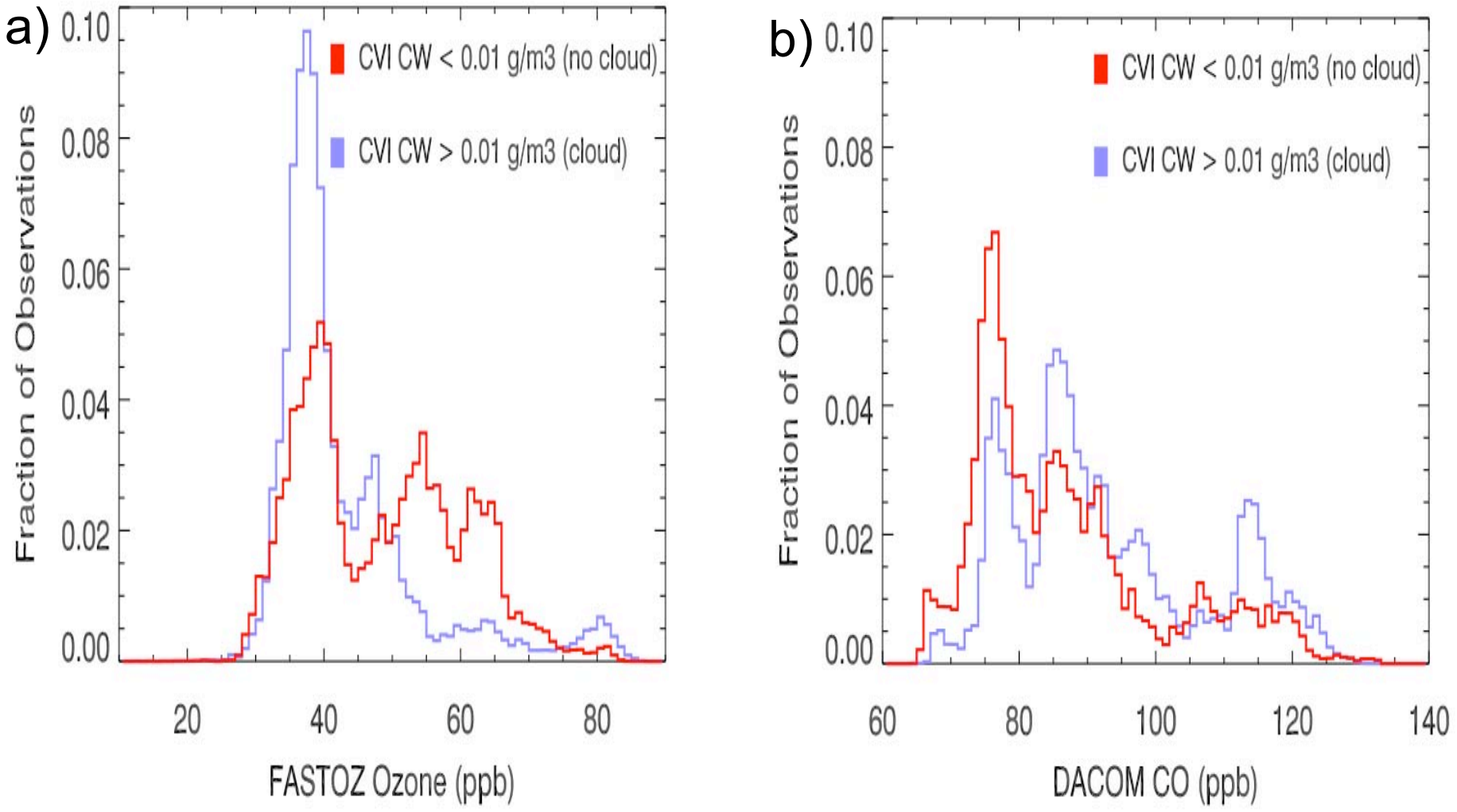

Figure 13

a) Probability of O_3 < 44 ppbv

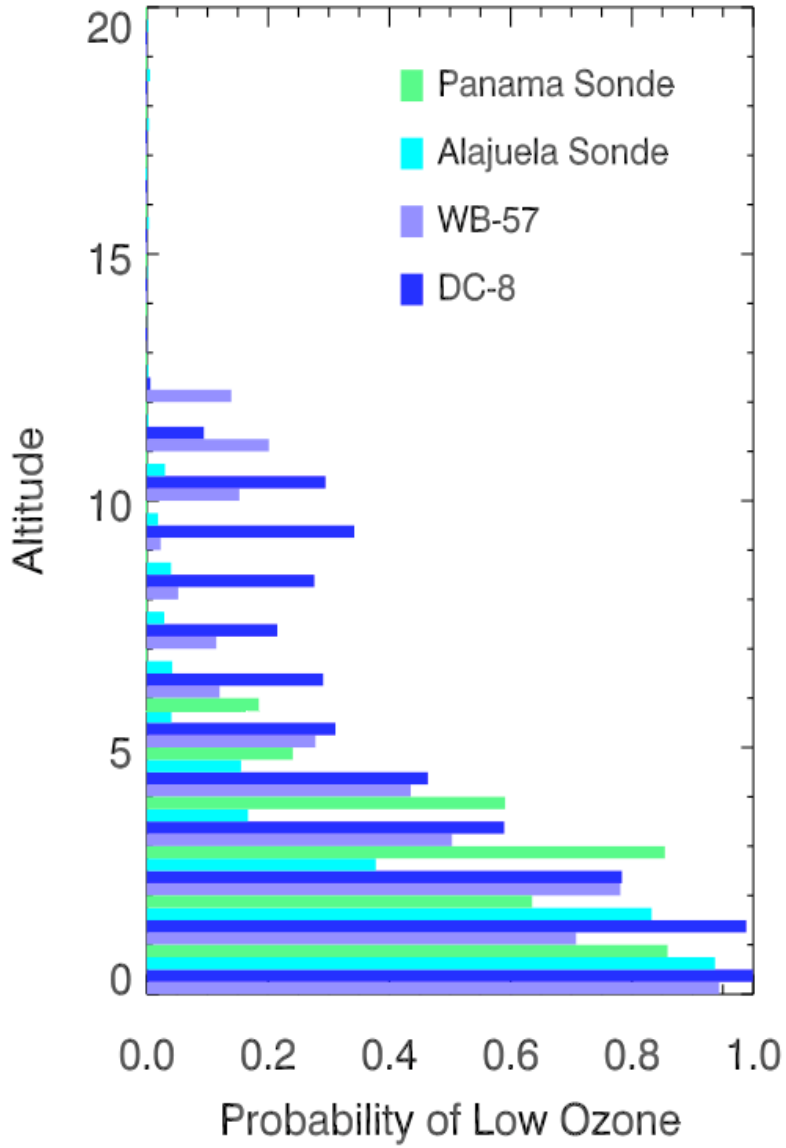

b) Probability of O_3 < 28 ppbv

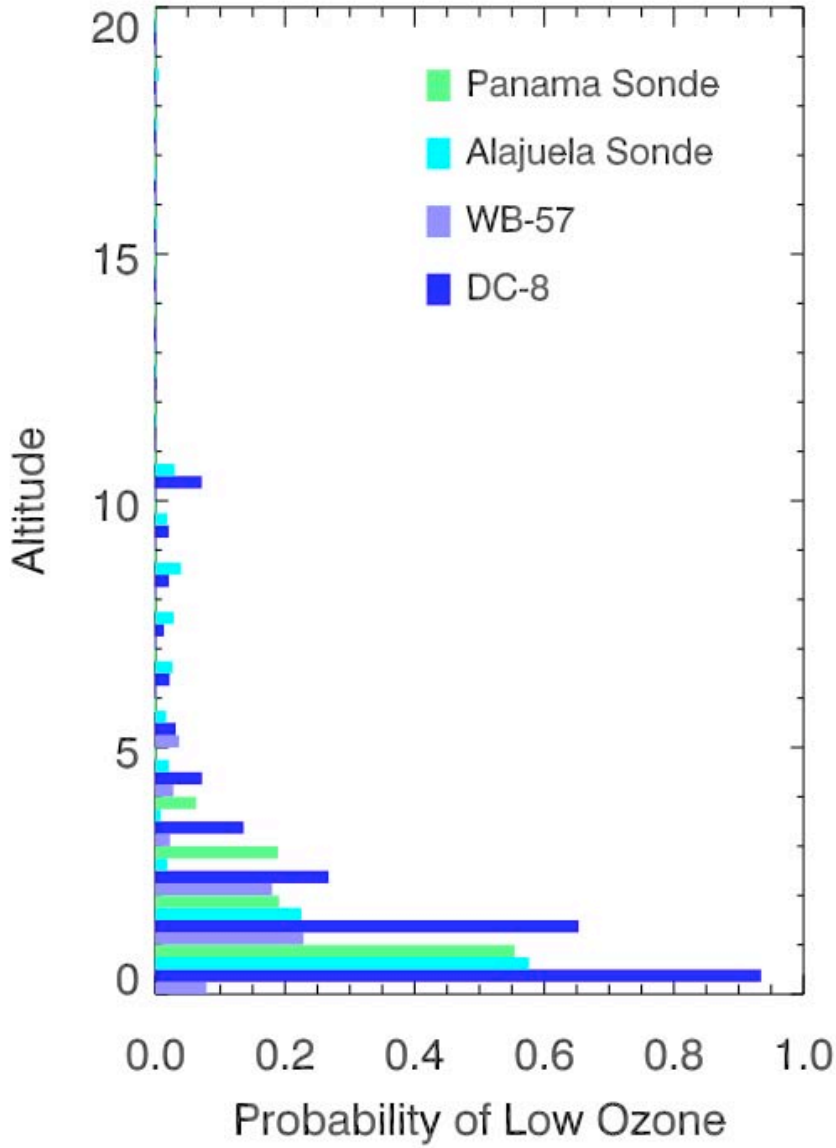

Figure 14

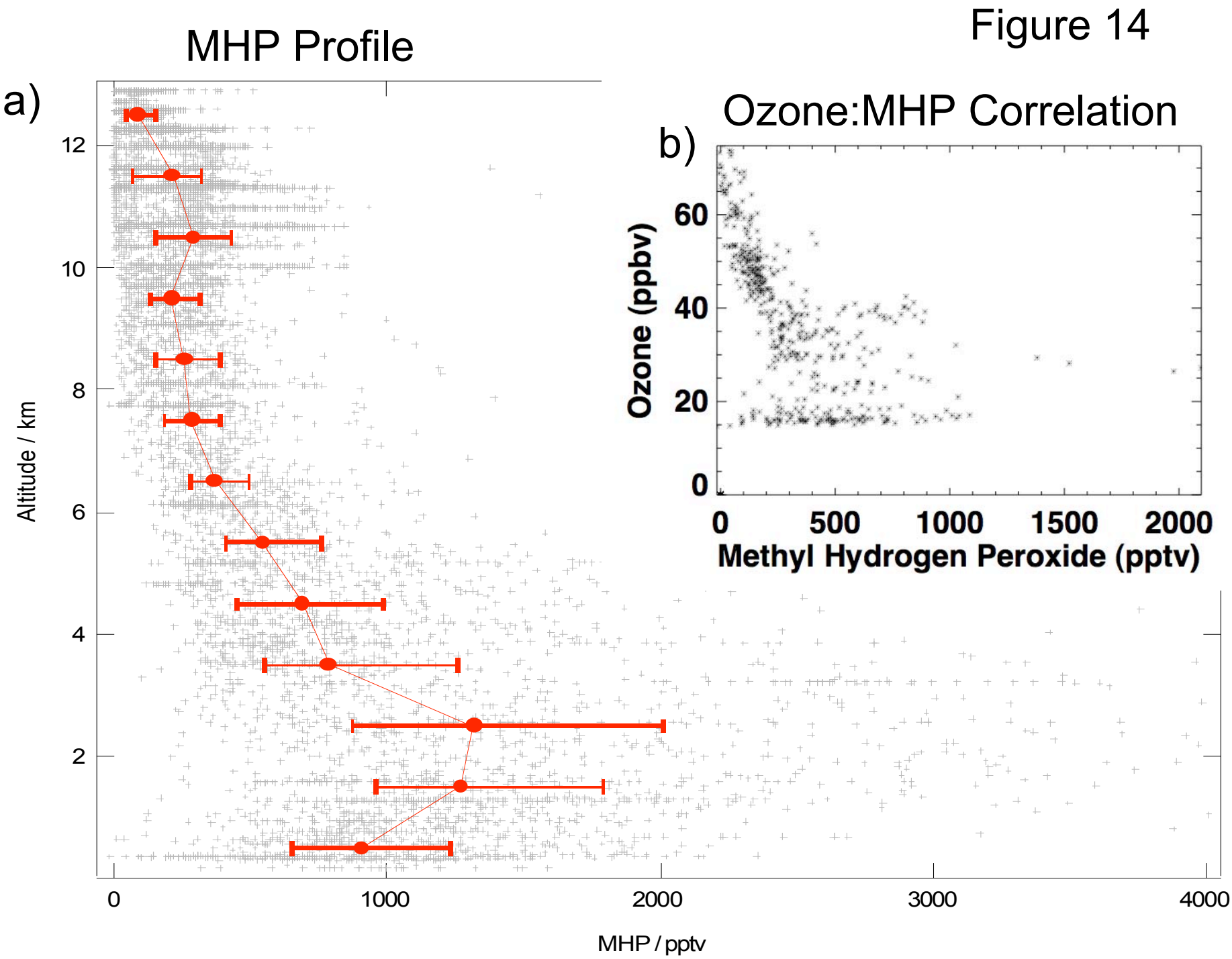
MHP Profile
a)
Altitude / km
12
10
8
6
4
2
0
1000
2000
3000
4000
MHP / pptv
Ozone:MHP Correlation
b)
Ozone (ppbv)
60
40
20
0
0
500
1000
1500
2000
Methyl Hydrogen Peroxide (pptv)

Figure 14

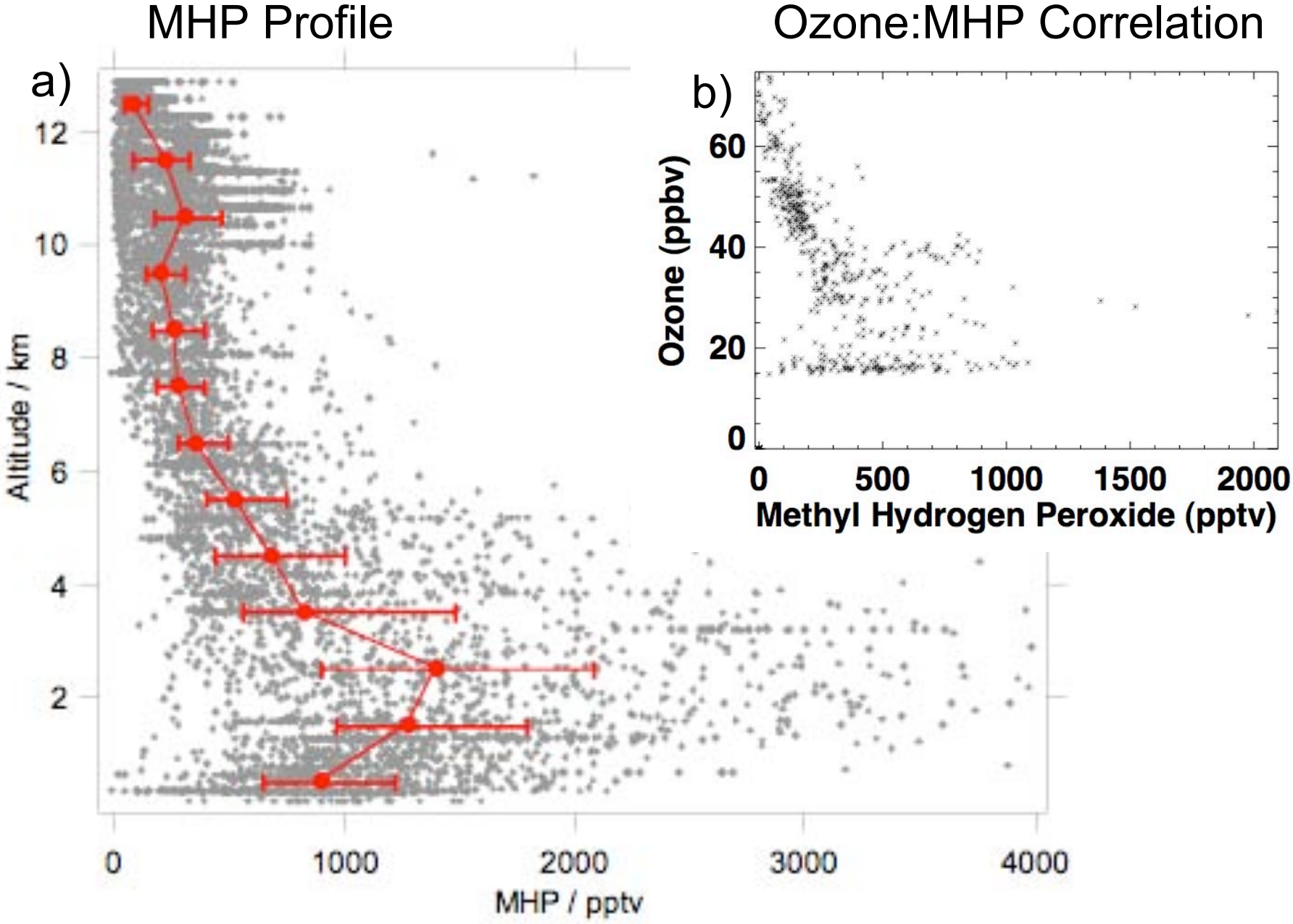
MHP Profile
Ozone:MHP Correlation
a)
b)
Altitude / km
MHP / pptv
Ozone (ppbv)
Methyl Hydrogen Peroxide (pptv)
0
2
4
6
8
10
12
1000
2000
3000
4000
20
40
60
500
1500

Figure 15

a) Total Organic Bromine Vertical Profile During TC4

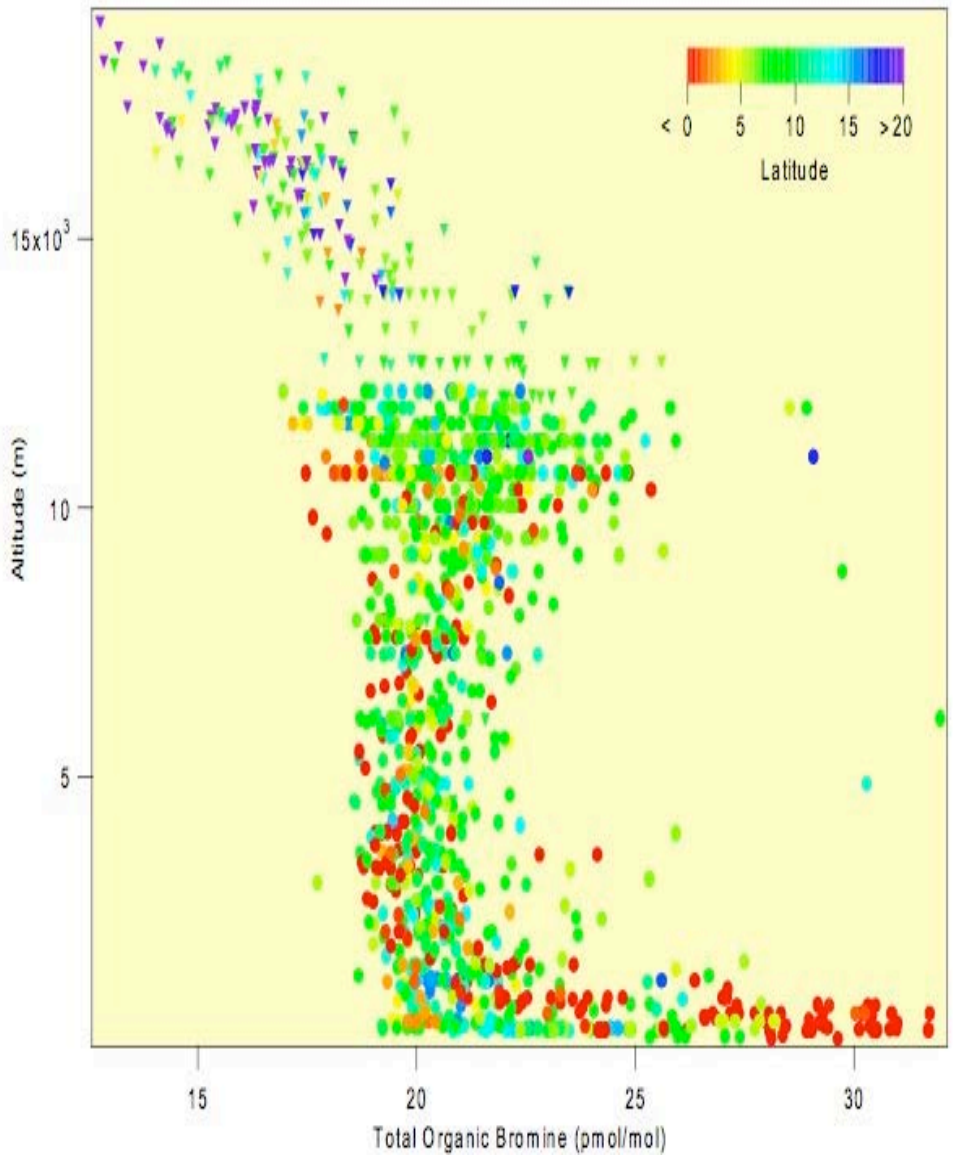

b) Aggregate Calcium Profile